A-16 ELASTO-PLASTIC STRESSES AND STRAINS IN CRACKED PLATES

J.L. Swedlow+*, M.L. Williams+** and W.H. Yang+***

ABSTRACT

A numerical method for analyzing the stresses and strains in work-hardening plates is applied to three crack problems. The first problem is that of an internally cracked plate, the second allows for reduced work-hardening, and the third involves external cracks. Selected data are presented and discussed briefly. One important result indicates that, compared to the elastic solution, the singularity of stress at the crack point decreases with load, while that for strain increases. Also, there are significant differences between internally and externally cracked plates in terms of the stress and strain fields.

+ Firestone Flight Sciences Laboratory, Graduate Aeronautical Laboratories, California Institute of Technology, Pasadena, California U.S.A.

* Research Fellow

** Professor of Aeronautics; presently Professor of Engineering, University of Utah, Salt Lake City, Utah

*** Research Fellow; presently Assistant Professor of Engineering Mechanics, University of Michigan, Ann Arbor, Michigan

Introduction

Over half a century ago, Inglis[1] deduced the elastic stress and strain fields in a plate containing a perfectly sharp crack. Among other things, he showed that the stress concentration at the crack point is infinite. While this result exceeds the limitations of elasticity, it nonetheless has provided a foundation for modern fracture mechanics. In discussing this classic work, Hopkinson[2] pointed out that the next step would be to repeat the analysis, allowing for both elastic and inelastic behavior.

Considerable progress has been made in this direction in recent years. For the most part, however, the various efforts reported in the literature* have involved certain idealizations, e.g., perfect plasticity, whose import is not readily evaluated. Comparison with experimental results indicates, however, that the detailed shape of the stress-strain curve is important.[7-11] What is needed, therefore, is a method of analysis that may be used with arbitrary stress-strain curves. In particular, we should be able to handle arbitrary work-hardening in treating crack geometries.

There is no great difficulty in establishing the field equations, at least within the context of mathematical plasticity. Beginning with the well-known Prandtl-Reuss flow rule,[12] the theory gives equations relating increments in stress and strain afforded by increments of applied load. See the Appendix. For plane stress (in the x-y plane), the constitutive relations may be shown[13] to take the form

$$
\begin{aligned}
E\delta\epsilon_x &= \delta\sigma_x - \nu\delta\sigma_y + (2\sigma_x - \sigma_y)\delta S \\
E\delta\epsilon_y &= \delta\sigma_y - \nu\delta\sigma_x + (2\sigma_y - \sigma_x)\delta S \\
E\delta\epsilon_{xy} &= (1+\nu)\delta\tau_{xy} + 3\tau_{xy}\delta S
\end{aligned}
\qquad (1)
$$

where E is the tensile modulus, ν is Poisson's ratio, and δ signifies an increment. Furthermore

$$
\begin{aligned}
\delta S &= \frac{E\delta\tau_o}{6\tau_o M_T(\tau_o)} \\
\tau_o &= \sqrt{2(\sigma_x^2 - \sigma_x\sigma_y + \sigma_y^2 + 3\tau_{xy}^2)}\Big/3 \\
\delta\tau_o &= \left[(2\sigma_x - \sigma_y)\delta\sigma_x + (2\sigma_y - \sigma_x)\delta\sigma_y + 6\tau_{xy}\delta\tau_{xy}\right]\Big/9\tau_o
\end{aligned}
\qquad (2)
$$

* See, e.g., Refs. 3-6.

and $M_T(\tau_o)$ is the tangent modulus of an octahedral stress-octahedral plastic strain curve, expressed as a function of the octahedral stress τ_o. To these relations are added the requirements of equilibrium and compatibility.

Because each of the stress and strain components is in effect the running sum of its increments, equations 1 and 2 are highly nonlinear. Upon closer inspection, however, it is seen that these relations are, to the first order, linear in the increments of their variables. Thus we may view a boundary-value problem as consisting of a set of quasi-linear sub-problems to be solved in succession. Each sub-problem is defined by the associated load increment and the accumulated values of the stresses. In substance therefore, we have a series of problems in linear, anisotropic, inhomogeneous elasticity.

It follows that any solution technique applicable to the latter class of problem may be extended to planar elasto-plasticity. In particular, certain well-developed numerical methods may be adapted, the primary modification being inclusion of all terms shown in equation 1.

Thus the elements of the requisite solution technique are readily available; it is necessary only to assemble them. This has been accomplished and a number of problems have been treated. For the present, we have selected $M_T(\tau_o)$ in a simple form* based on the Ramberg-Osgood formula:

$$
\frac{E}{M_T(\tau_o)} = \begin{cases} 0, & \tau_o \le \tau_\ell \\ \dfrac{2E\epsilon_y}{n\tau_\ell}\left(\dfrac{\tau_o}{\tau_\ell} - 1\right)^{1/n-1}, & \tau_o > \tau_\ell \end{cases}
\qquad (3)
$$

where ϵ_y is a constant, τ_ℓ is the octahedral stress at the proportional limit, and $0 < n < 1$ is a constant. The numerical technique we have used is known, for elastic analysis, as the direct stiffness method.[14]

With the solution technique thus assembled, we have begun study of a series of boundary-value problems of interest in fracture mechanics. The present paper reports certain results for an arbitrarily selected stress-strain curve and plate geometry, together with some variations. Attention is limited to increasing load; unloading phenomena are deferred to a subsequent report.

Problem Specifications

The first, or reference, problem considered is that of a rectangular plate containing a centrally placed internal crack. The half-crack length is taken as unity; length and width of the plate are nine and six, respectively. The plate is loaded in uniaxial tension perpendicular to the line of the crack, instantaneous stress $\bar{\sigma}$ being accumulated

* The present analysis will easily accomodate other representations for the tangent modulus, providing the stress-curve is monotonic.

from a succession of increments. See Table 1. Due to the symmetry of the problem, only one quadrant of the plate was analyzed. This quadrant is represented by a total of 348 triangular elements of varying size and shape; the elements are joined at 200 nodes. The smallest elements are located in the vicinity of the crack point and have a characteristic dimension of 0.05, referred to the half-crack length. See Figures 1a, b, c. The boundary conditions are:

$$
\left.\begin{array}{lll}
x = 3.0: & \sigma_x = \tau_{xy} = 0 \\
y = 4.5: & \tau_{xy} = 0 \\
 & \sigma_y = \bar{\sigma} \\
x = 0.0: & \tau_{xy} = 0 \\
 & u = 0 \\
y = 0.0: & \tau_{xy} = 0 \\
x < 1.0: & \sigma_y = 0 \\
x \geq 1.0: & v = 0
\end{array}\right\} \qquad (4)
$$

where u and v are the x- and y- components of the displacement vector, respectively.

The material properties and constants (eqn 3) are:

$$
\begin{aligned}
E &= 10.80 \times 10^6 \text{ lb/in}^2 \\
\nu &= 0.3333 \\
\varepsilon_y &= 0.009716 \\
n &= 0.3964 \qquad (5) \\
\tau_\ell &= \sqrt{2}\,\sigma_\ell/3 \\
\sigma_\ell &= 11.50 \times 10^3 \text{ lb/in}^2
\end{aligned}
$$

and the resulting curve is shown in Figure 2. Consistent with the use of finite load increments, the continuous stress-strain curve was replaced by a series of points such that the actual curve traversed by each element is multi-linear, i.e., a series of connected line segments.

Deviation from the actual curve and the actual slope (tangent modulus) is controlled by proper selection of these points.

The second problem is identical to the first in all respects except one. In order to reduce the work-hardening, ε_y was increased by 50% to the value 0.01457. The resulting curve is shown in Figure 2.

The third problem represents a geometric inversion of the first in that the boundary conditions at x = 0.0 and x = 3.0 are interchanged, giving a plate with symmetric edge cracks. The crack length/plate width ratio is maintained, and the relative arrangement of elements in Figures 1b and c is unchanged. Material properties are specified by equation 5.

Summary of Results

In each problem, the first load increment is adjusted to bring the most highly stressed element slightly above the proportional limit, and the solution corresponds to that of classical elasticity. Subsequent increments of $\bar{\sigma}$ occur in the presence of some inelastic behavior -- see Table 1. Following each load increment, the displacements, strains, stresses, and energy densities for each node or element are computed; a total of 1.1×10^5 pieces of data are printed out for each case. In order to conserve space, we show selected data pertinent to fracture mechanics.

It is convenient to present data graphically, for which we employ several techniques. One is to show the spatial distribution of a quantity along a given line and another, the spatial distribution over an area using contour lines, i.e., lines along which the quantity assumes a fixed value. We also examine the variation of a given quantity at a fixed point as the load increases. The last technique, while not meaningful for linear elasticity, illuminates certain aspects of elasto-plastic flow.

We show first the stress and strain fields produced by the initial load increment, comparing them to results obtained from classical planar theory. For example, Figure 3 shows the value of $\sigma_y/\bar{\sigma}$ along the x-axis* obtained numerically and from Inglis' solution for the infinite plate.** It is apparent that the computational technique used,

* Actually, the computer program in its present version does not give point values of the stresses or strains. Instead, values refer to an entire element and are thus 'averaged' over the area covered by that element. Since no element straddles the x-axis, the values apply slightly above the axis. We have referred these to points defined by the centroid of each triangle, the justification being agreement with analytic results. As pointed out in Ref. 15, other representations might be more consistent with the spirit of finite element methods. In our case, however, the resolution of meshes seems to be sufficient so that use of point values is appropriate.

** While more precise comparison could perhaps be made with a finite plate solution, e.g., Ref. 16, the Inglis solution is sufficient for evaluation near the crack. Comparison is made only for an internal crack.

together with the element configuration, is capable of resolving reasonably high stress concentrations. A finer mesh at the crack tip would presumably show even higher concentrations. Moreover, the agreement between numerical and analytic results is adequate, except perhaps immediately behind the crack point. The y-coordinates of these few points are comparable to that of their x-coordinate, and they cannot be regarded as close to the x-axis. In this connection, it may be noted that the high gradients in this area proved to be a severe test for the resolving power of the elements.

A similar comparison might be made for the strains, but since the elastic strains and stresses are linearly related, the same correspondence is to be expected. Of more interest is the distribution of maximum shear strain around the crack point, as shown in Figure 4, in comparison with the infinite plate solution (internal crack). It is seen that corresponding contours do not fall along one another, but the presence of finite boundaries in the one solution precludes much closer agreement. The difference follows the trend shown by Redshaw and Rushton[17] and to that extent, accuracy of the numerical solution is deemed satisfactory.

Further Loading: Increasing the loading causes local yielding which spreads over the plate. As, for example, elements along the x-axis yield, their load-carrying capacity is reduced and successive elements will become more highly stressed. This is illustrated by the variation of σ_y for the six elements ahead of the crack. In Figure 5a we show $\sigma_y/\bar{\sigma}$ for the reference problem, the purpose of non-dimensionalization being to show deviation from proportional loading.* At low loads, the stresses remain in fixed ratios to one another. At a certain point these ratios begin to change, due to yielding of more highly stressed elements. The precise load at which this deviation occurs depends of course on the configuration of the elements, but the agreement shown in Figure 3 suggests the actual value is given reasonably well by the present calculation.

In turn, each of the elements yields, shown by the maxima of the curves in Figure 5a. The values of $\sigma_y/\bar{\sigma}$ drop more or less sharply; subsequently the curves flatten out. These elements are in a condition of proportional loading up to the point at which yielding occurs. This is followed by a transition, leading to a phase of quasi-proportional loading. Most of the load redistribution can be associated with this transition, with only minor changes occurring thereafter. In a sense, the transition is also associated with the "knee" of the stress-strain curve, and the next phase with the much flatter portion beyond.

It should be evident that the same processes will occur at any point loaded into the plastic region. The extent of load redistribution

* These data are shown as smooth curves rather than discrete points. Scatter of the points was found to be hardly more than the width of the line used.

perforce depends upon the details of the stress-strain curve. In particular, a significant portion of the loading history is incorporated into the transition phase, and the nature of initial yielding will have a dominant influence on the stress and strain states prior to fracture.*

Similar data are shown in Figure 5b for the second and third problems. This particular method of changing work-hardening does not affect the stress field noticeably, probably because all stress-based quantities have been held fixed. The strain field, as shown below, is altered by this change in work-hardening. Concentration of stress is slightly higher in the externally cracked plate, following a trend observed in the analytic solution.[18]

Singular Behavior: Of some interest is the singular behavior of the stresses. From planar elasticity we have

$$\sigma_x + \sigma_y\Big|_{y=0} = K\bar{\sigma}\,[(x-b)/2b]^{-\frac{1}{2}} + O(x/b) \qquad (6)$$

where b is the half-crack length, and K is a constant. With the present method we cannot of course obtain singular quantities, but we may use some of the data to compute an indicated stress singularity. We first rewrite equation 6 in the form

$$\sigma_x + \sigma_y\Big|_{y=0} \doteq K(\bar{\sigma})\bar{\sigma}\,[(x-b)/2b]^{n(\bar{\sigma})} \qquad (7)$$

Next we evaluate $K(\sigma)$ and $n(\sigma)$ from a least squares fit of the data at elements 6, 26, 50, and 77. For the first (elastic) load increment, we find for the internal crack

$$K_{elastic} = 1.19$$
$$n_{elastic} = -0.51 \qquad (8a)$$

Values for the external crack are**

$$K_{elastic} = 1.48$$
$$n_{elastic} = -0.48 \qquad (8b)$$

* This same observation may be made of the data shown in Refs. 8 and 10.

** Appropriate reversal of the x-coordinate has been made.

In both cases, deviation ≈ 0.01. The indicated singularity is slightly lower for the external crack case, but the indicated elastic stress intensity is nearly 25% higher. As loading is increased, these parameters vary as shown in Figures 6a and b. The three phases noted above manifest themselves in both curves. Not only does the intensity of the indicated stress intensity vary with load, but also the strength of the singularity itself. Respective behavior of internal and external cracks is maintained throughout the loading sequence.

The strains exhibit a related behavior. In the same manner as above we write

$$\left.\frac{E(\varepsilon_x + \varepsilon_y)}{1 - \nu}\right|_{y=0} \doteq K(\bar{\sigma})\bar{\sigma}\,[(x-b)/2b]^{n(\bar{\sigma})} \qquad (9)$$

and evaluate $K(\bar{\sigma})$ and $n(\bar{\sigma})$. Eq. 9 is written so that equations 8a, b obtain; subsequent dependence is given in Figures 7a and b. The trend is noticeably different here. The indicated strain intensity factor increases sharply, and the strength of the indicated singularity increases with some suggestion of a limiting value. Again, some differences are to be noted between the internal and external crack geometries.

Plastic Enclave Growth: For the arrangement of elements shown in Figure 1, there is no plastic enclave for $\bar{\sigma} < 2300$ lb/in^2. As load increases, however, yielding occurs and sizable plastic zones are generated. Consistent with the distinction between elastic and elasto plastic flow used in this computation -- see Eq. 3 -- we define the plastic enclave as that contour along which $\tau_o/\tau_\ell = 1$. This definition does not of necessity depend upon the recoverability of strain, that is, elastic strains are physically defined as those which are recovered after load removal, and may not be equivalent to simple linearity between stress and strain. The difference in these two definitions is non-trivial for the stress-strain curve used in this analysis. This may be seen by finding the value of τ_o/τ_ℓ at the proportional limit and, say, the 0.2% offset. These two values are 1.0 and 1.47, respectively, for $\varepsilon_y = 0.009\ldots$, and a slight offset corresponds to a large increase in yield stress. As a result, delineation of the plastic enclave in terms of τ_o/τ_ℓ will be a sensitive function of the specific numerical value of this ratio actually used.

With this qualification in mind, we may examine the growth of the plastic enclaves, shown in Figure 8 for the reference problem. At an applied stress less than about 9,000 lb/in^2, the yielded zone is contained by material still in the linear elastic range, making the term plastic enclave quite appropriate. At $\bar{\sigma} \approx 10,000$ lb/in^2, the plastic zone intersects the free edge, and at 11,500 lb/in^2 (the proportional limit), the plastic zone includes a small portion of the loaded edge. At still higher loads, the boundary moves to the y-axis, and in effect an elastic enclave is generated. Because the plastic enclave is defined in terms of a stress, its growth is not greatly influenced by the reduction in work-hardening of the second problem. We therefore omit a detailed plot. The externally cracked plate, however, shows different enclave growth patterns, as

may be seen in Figure 9. The enclaves are more nearly erect at lower loads. At $\bar{\sigma} \approx 10,000$ lb/in^2, when enclaves in the internally cracked plate have reached the free edge, those for the third problem join along the y-axis. In addition to being contained by an elastic area, the plastic enclaves surround an inner elastic zone. When $\bar{\sigma}$ reaches the proportional limit, a greater portion of the externally cracked plate has yielded, at least in terms of the present definition. Hence it would appear that the rate of growth is greater in externally cracked plates than those with an internal crack.

Strain Fields: An indication of the distribution of strain is given by contours of the difference between the principal strains. This quantity is proportional to the maximum shear strain, and these contours are therefore similar to isochromatic fringes observed in photoelastic experiments. For the reference problem, these contours are plotted in Figures 10 and 11 for $\bar{\sigma} = 8,000$ lb/in^2 and 13,000 lb/in^2. Selected contours for all three problems are shown in Figures 12 and 13. It is seen that reduction of work-hardening tends to produce narrower, less erect shapes, while inversion of the crack geometry gives a higher concentration of strain at the crack point.

Strain Energy: The strain energy density at any point of the plate is given by

$$W = \frac{1 - 2\nu}{6E}(\sigma_x + \sigma_y)^2 + \frac{3(1+\nu)}{2E}\tau_o^2 + \frac{3}{2}\int_o^{\tau_o} \frac{\xi\, d\xi}{M_T(\xi)} \qquad (10)$$

The first two terms on the right of Eq. 10 represent the linear elastic portion of W, and may be regarded as dilatational and distortional, respectively, in the usual sense. The last term gives the inelastic strain energy density and is solely distortional because there is no plastic dilatation. If W is integrated over the plate area, we have the total strain energy (per unit thickness) in the plate and can separate the elastic and plastic portions. This has been done and the results are shown in Figure 14 for the three problems under consideration. It is seen that the elastic energies for all three are nearly the same, primarily a result of having held stress-based quantities fixed. Noticeable differences occur, however, in the plastic portion of the strain energy. The externally cracked plate absorbs less work than the other two, a result of the more localized strain concentrations.

Discussion

The results presented in this paper are selections from extensive data generated by a newly-developed solution technique for elasto-plastic plates. The objective has been to produce these results without recourse to ad hoc assumptions for specialized geometries, e.g., cracks, and this objective seems to have been met. Further development of the

technique might involve its application to a particular problem for which experimental data are available. Detailed comparison between physical and analytical results could then be used for more extensive evaluation of the technique.

The work to date, based on the idealized representation of M_T in Eq. 3, has provided considerable information as to the nature of any experiment intended for comparison. For example, it is clear that specification of the stress-strain curve must be very accurate, particularly in the region of initial yielding. The experiment should be also designed to detect characteristics such as loading phases and indicated stress and strain singularities.

Fracture Criterion: Ultimately we are interested in using this analysis to deduce a critical value of the applied stress, i.e., the point at which the crack begins to extend. The question arises, how should the results be used to achieve this end? There is, unfortunately, no clear answer and in fact, this matter is the subject of considerable study.

In a broad sense, two types of condition are available. The first is based on the concept of limiting values of some field quantity. For example one might argue bounds on maximum stress or strain, dilatation, distortion, energy density, etc. In any event, criteria of this type pertain to phenomena at a point, presumably at or near the crack tip. Therefore, considerably more information than is now available is required as to the details of the stress and strain fields and the limiting behavior of the material.

The second type of condition deals with stability of the crack geometry, considered as a part of an overall system. In the special case of linear elasticity, such a condition reduces to the well-known Griffith criterion. The primary requirement, which stems from the first law of thermodynamics, is that the potential energy of the loaded plate remains stationary during an infinitesimal extension of the crack.

Note that this is not equivalent to the equality in energy of two plates similarly loaded but having crack lengths differing by an infinitesimal amount. It is crucial that we allow for a stress relaxation in the neighborhood of the crack front during the process of extension. The material immediately ahead of the crack, at its original length, is subject to a stress reversal during extension, and the associated change in elastic and plastic energies cannot be computed from the results of simple loading analyses such as are presented above.

The first step in computing an energetic fracture criterion is therefore an unloading analysis. For this we need a complete prescription of the stress-strain curve and, to be accurate, details such as hysteresis and Bauschinger effect ought to be included. This is evidently analogous to the need for details of the stress-strain curve in the region of initial yielding, and may be as difficult to obtain in the laboratory.

Acknowledgments

Work reviewed in this paper was supported by the Air Force Materials Laboratory under Contract AF 33(615)-2186. Computations were performed at the Willis H. Booth Computing Center, California Institute of Technology. The authors are pleased to acknowledge the cooperation of Professor C. W. McCormick, Jr. and Mr. K. J. Hebert in providing a portion of the computational methods.

REFERENCES

1. Inglis, C. E., Transactions of the Institute of Naval Architects (London), 60, 1913, 11. 219-230.

2. Hopkinson, B., Transactions of the Institute of Naval Architects (London), 60, 1913, 11. 232-234.

3. Allen, D. N. de G. and Southwell, R. V., Philosophical Transactions of the Royal Society (London), series A, 242, 1949-50, pp. 379-414.

4. Jacobs, J. A., Philosophical Magazine, 41, 1950, pp. 349-361.

5. Stimpson, L. D. and Eaton, D. M., ARL 24, Aerospace Research Laboratories, Office of Aerospace Research, Wright-Patterson Air Force Base, July 1961 (ASTIA AD 266 347).
See also extracted results in: Williams, M. L., Proceedings of the Crack Propagation Symposium, 1, College of Aeronautics, Cranfield (England), September 1961, 11. 130-165.

6. Hendrickson, J. A., Ph.D. Dissertation, California Institute of Technology, 1957.

7. Dugdale, D. S., Journal of the Mechanics and Physics of Solids, 8, 1960, 11. 100-104.

8. Dixon, J. R., and Strannigan, J. S., NEL Report No. 115, National Engineering Laboratory (Scotland), October 1963.

9. Ault, R. T. and Spretnak, J. W., ASD-TDR-62-223, Directorate of Materials and Processes, Aeronautical Systems Division, Wright-Patterson Air Force Base, April 1962.

10. Gerberich, W. W., Experimental Mechanics, 4, 11, November 1964, pp. 335-344.

11. Swedlow, J. L. and Gerberich, W. W., Experimental Mechanics, 4, 12, December 1964, pp. 345-351.

12. Hill, R., The Mathematical Theory of Plasticity, Oxford University Press, 1950.

13. Swedlow, J. L. and Yang, W. H., GALCIT SM 65-10, California Institute of Technology, May 1965.

14. Turner, M. J., Clough, R. W., Martin, H. C., and Topp, L. J., Journal of Aeronautical Sciences, 23, 9, September 1956, pp. 805-823, p. 854.

15. Percy, J. H., Loden, W. A., and Navaratna, D. R., RTD-TDR-63-4032, AF Flight Dynamics Laboratory, Wright-Patterson Air Force Base, October 1963.

16. Sneddon, I. N., The Effect of Internal Cracks on the Distribution of Stress in Thin Elastic Strips and Cylinders, Applied Mathematics Research Group, North Carolina State College, July 1963.

17. Redshaw, S. C. and Rushton, K. R., Journal of the Mechanics and Physics of Solids, 8, pp. 173-186.

18. Swedlow, J. L. and Williams, M. L., ARL 64-175, Aerospace Research Laboratories, Office of Aerospace Research, Wright-Patterson Air Force Base, October 1964.

Appendix:

The constitutive relations for elasto-plastic flow theory are derived as indicated in the following brief outline. Each strain increment is separated into elastic and plastic parts, viz.,

$$\delta\varepsilon_{ij} = \delta\varepsilon_{ij}^{(e)} + \delta\varepsilon_{ij}^{(p)} \tag{11}$$

The elastic portion is required to follow the generalized Hookean Law

$$\delta\varepsilon_{ij}^{(e)} = \frac{1-2\nu}{E}(\delta\sigma_{kk})\delta_{ij} + \frac{1+\nu}{E}\delta s_{ij} \tag{12}$$

where

$$\delta s_{ij} = \delta\sigma_{ij} - (\delta\sigma_{kk})\delta_{ij}/3 \tag{13}$$

is the deviator of the rate of stress tensor, and δ_{ij} is the Kronecker delta. We use indicial notation and its associated conventions. Latin indices have the range 1, 2, 3.

The plastic strain rate is assumed to obey the Prandtl-Reuss flow rule

$$\delta\varepsilon_{ij}^{(p)} = s_{ij}\,\delta\lambda \tag{14}$$

where s_{ij} bears the same relation to σ_{ij} as δs_{ij} to $\delta\sigma_{ij}$, and $\delta\lambda$ is a positive scalar function. If we multiply Eq. 14 by itself we find

$$\delta\lambda = (\delta\varepsilon_{ij}^{(p)}\,\delta\varepsilon_{ij}^{(p)})^{\frac{1}{2}}/(s_{k\ell}\,s_{k\ell})^{\frac{1}{2}} \tag{15}$$

For convenience we define the octahedral plastic strain rate

$$\delta\varepsilon_o^{(p)} = (\delta\varepsilon_{ij}^{(p)}\,\delta\varepsilon_{ij}^{(p)}/3)^{\frac{1}{2}} \tag{16}$$

and the octahedral stress

$$\tau_o = (s_{ij}\,s_{ij}/3)^{\frac{1}{2}} \tag{17}$$

so that Eq. 15 becomes

$$\delta\varepsilon_{ij}^{(p)} = \frac{\delta\varepsilon_o^{(p)}}{\tau_o}\,s_{ij} \tag{18}$$

A uniaxial tensile test may be used to evaluate $\delta\varepsilon_o^{(p)}$ in terms of τ_o. It may be shown that the result is

$$\delta\varepsilon_o^{(p)} = \delta\tau_o/[2M_T(\tau_o)] \tag{19}$$

where $M_T(\tau_o)$ is the tangent modulus of the associated octahedral stress-octahedral plastic strain curve.

Combining these, the constitutive relations between the stress and strain rates are found to be

$$\delta\varepsilon_{ij} = D_{ijk\ell}\,\delta\sigma_{k\ell} \tag{20a}$$

where

$$D_{ijk\ell} = \frac{1+\nu}{2E}(\delta_{ik}\delta_{j\ell} + \delta_{i\ell}\delta_{jk}) + \frac{(\sigma_{ij} - \sigma_{pp}\delta_{ij}/3)(\sigma_{k\ell} - \sigma_{qq}\delta_{k\ell}/3)}{2M_T(\sigma_{mn} - \sigma_{rr}\delta_{mn}/3)(\sigma_{mn} - \sigma_{ss}\delta_{mn}/3)} \quad (20b)$$

In the case of plane stress, for which we associate the indices 1, 2, 3 with x, y, z, if is required that

$$\sigma_x = \sigma_x(x, y) \; ; \quad \tau_{xy} = \tau_{xy}(x, y)$$

$$\sigma_y = \sigma_y(x, y) \; ; \quad \tau_{xz} = \tau_{yz} = \sigma_z = 0 \quad (21)$$

Substitution of Eq. 21 into Eqns. 20 a and b leads directly to Eqns. 1 and 2.

Other specialized cases of Eqns. 20 may easily be derived, e.g., plane strain, torsion, axisymmetry. These relations may also be generalized to orthogonal curvilinear coordinates by means of appropriate tensor operations. A more detailed account of the foregoing derivation appears in Ref. 13.

TABLE 1

Increment No.	Load Increment	Accumulated Load
1	2,300 lb/in^2	2,300 lb/in^2
2	200	2,500
3	300	2,800
4	300	3,100
5	300	3,400
6	300	3,700
7	300	4,000
8	400	4,400
9	400	4,800
10	400	5,200
11	400	5,600
12	400	6,000
13	500	6,500
14	500	7,000
15	500	7,500
16	500	8,000
17	500	8,500
18	500	9,000
19	500	9,500
20	500	10,000
21	500	10,500
22	500	11,000
23	500	11,500
24	500	12,000
25	500	12,500
26	500	13,000

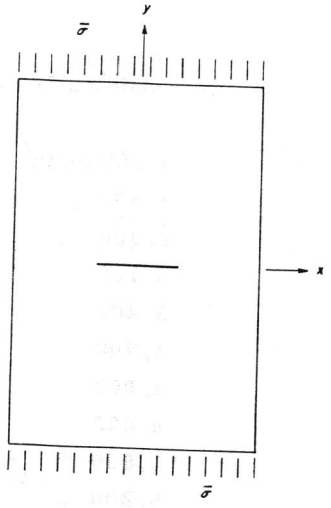

Fig. 1a

Geometry of internally cracked plate.

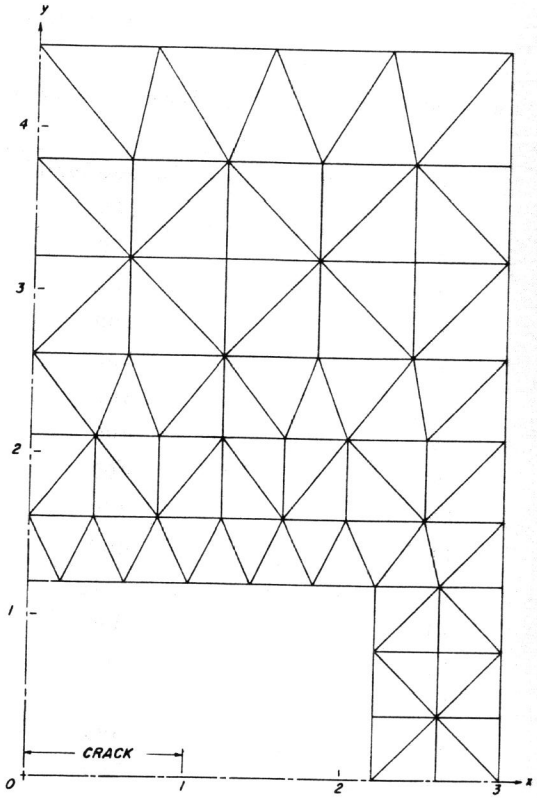

Fig. 1b

Finite element representation of first quadrant of plate. See Figure 1c for details near crack.

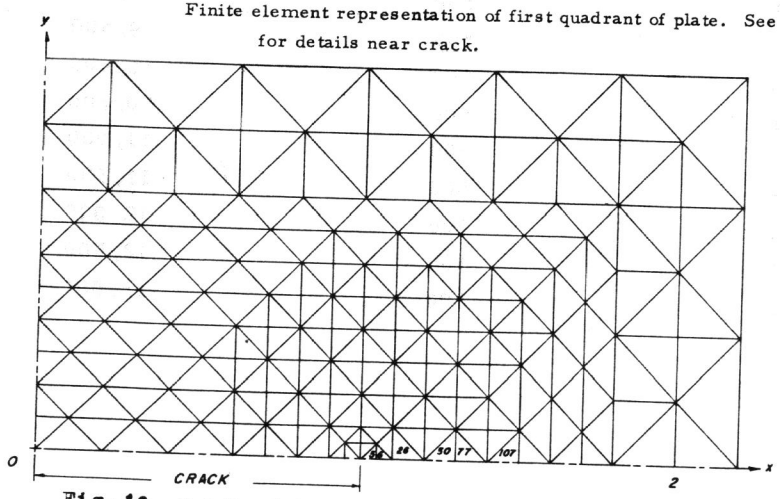

Fig. 1c Details of element configuration near the crack. Note position of numbered elements.

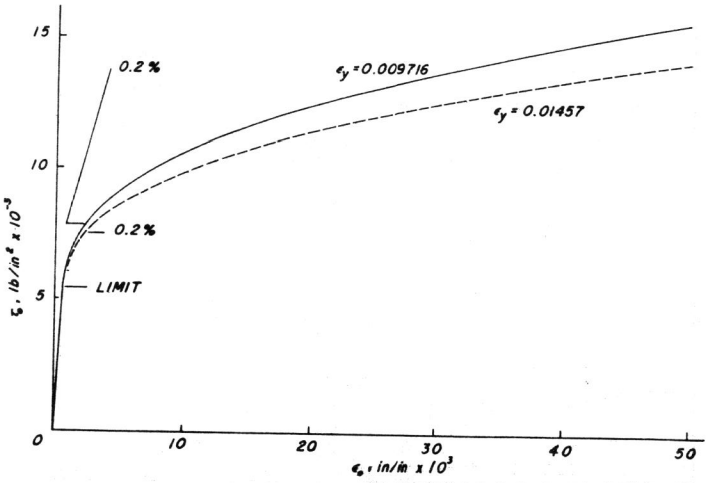

Fig. 2 Stress-strain curves used in analysis, based on eqns 3 and 5.

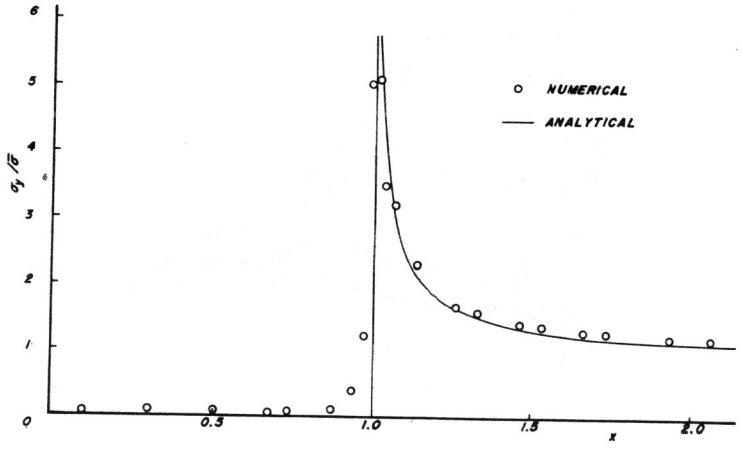

Fig. 3 Distribution of $\sigma_y/\bar{\sigma}$ along the x-axis, numerical results compared to Inglis' solution.

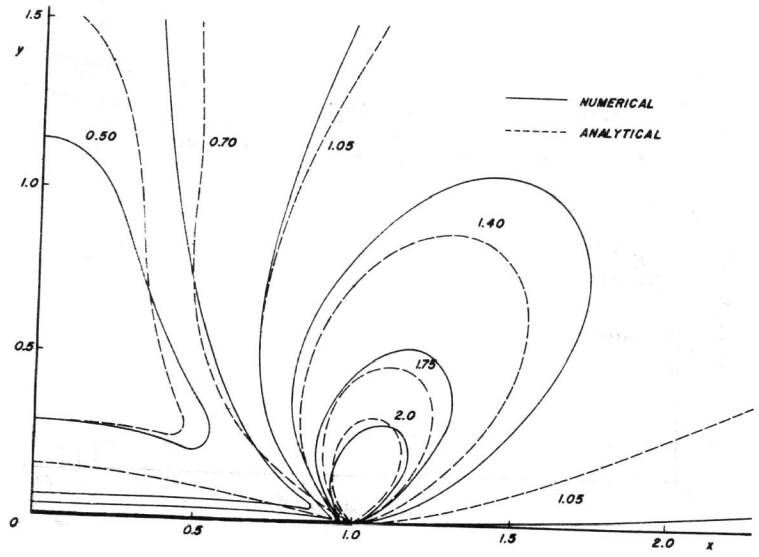

Fig. 4 Contours of $E(\varepsilon_1 - \varepsilon_2)/[(1+\nu)\bar{\sigma}]$, numerical results compared to Inglis' solution.

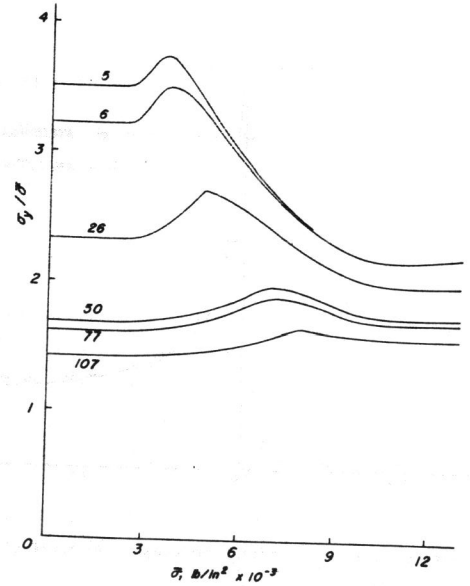

Fig. 5a Variation of $\sigma_y/\bar{\sigma}$ with $\bar{\sigma}$, six elements ahead of crack, reference problem.

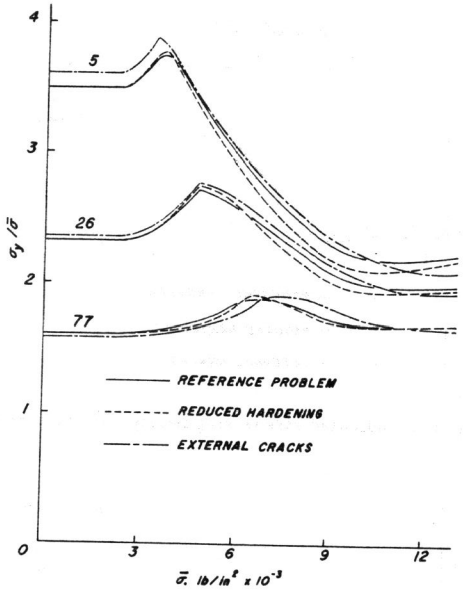

Fig. 5b Variation of $\sigma_y/\bar{\sigma}$ with $\bar{\sigma}$, selected elements ahead of crack, three problems.

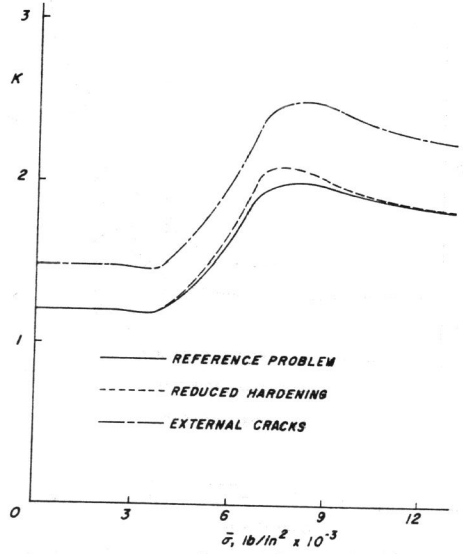

Fig. 6a Variation of indicated stress intensity with $\bar{\sigma}$, three problems.

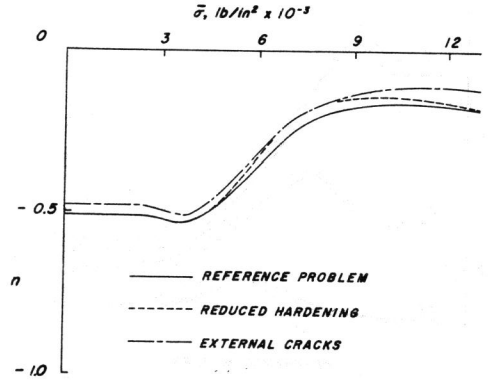

Fig. 6b Variation of indicated stress singularity with $\bar{\sigma}$, three problems.

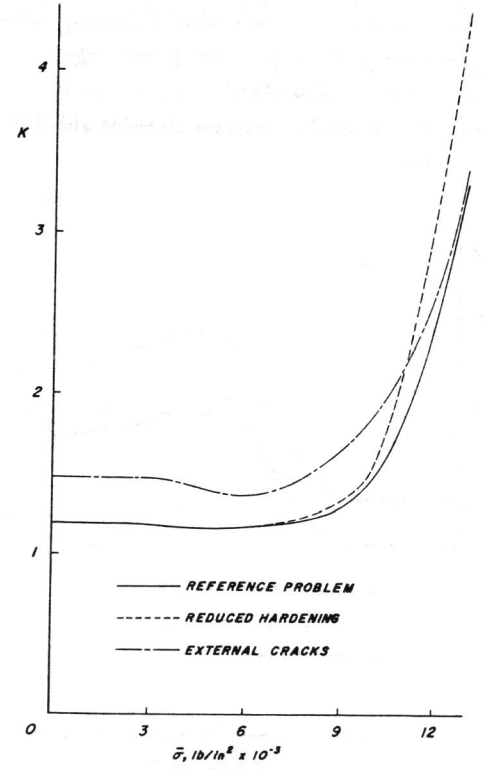

Fig. 7a Variation of indicated strain intensity with $\bar{\sigma}$, three problems.

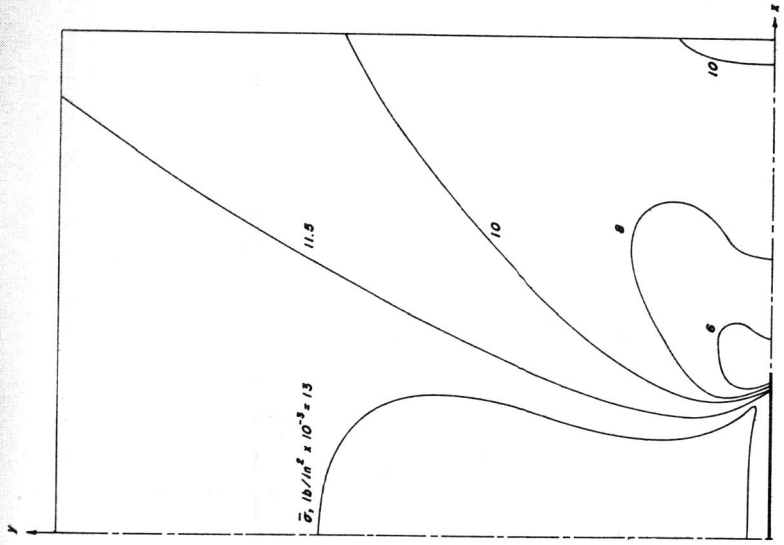

Fig. 8 Growth of the plastic enclave, reference problem.

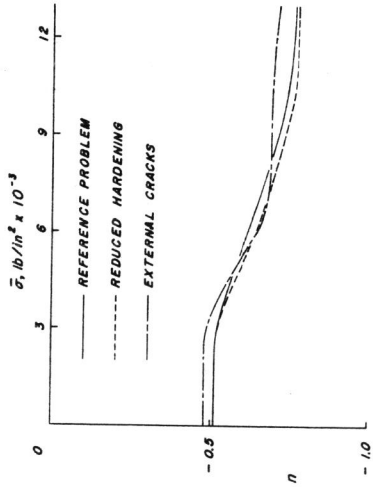

Fig. 7b Variation of indicated strain singularity with $\bar{\sigma}$, three problems.

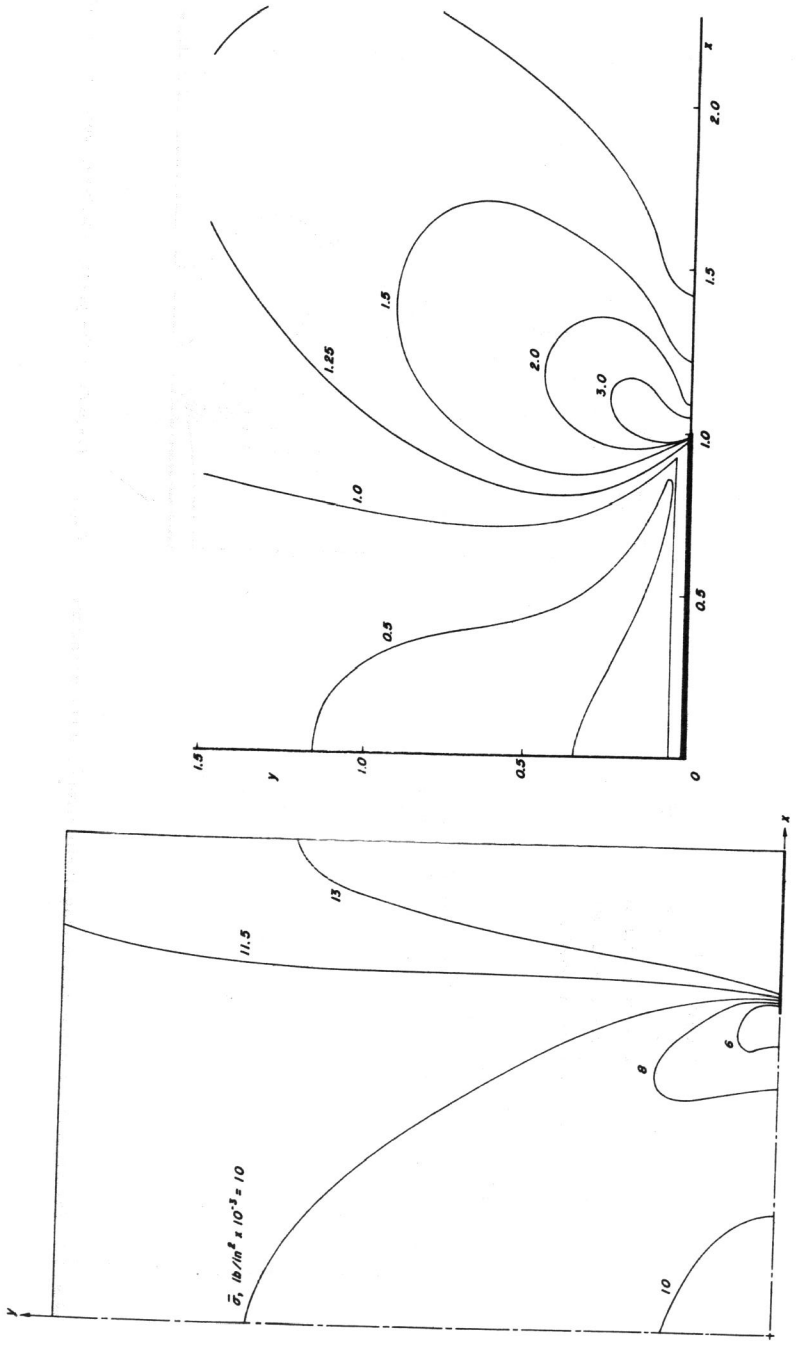

Fig. 9 Growth of the plastic enclave, external cracks.

Fig. 10 Contours of $(\epsilon_1 - \epsilon_2) \times 10^3$ at $\bar{\sigma} = 8 \times 10^3$ lb/in^2, reference problem.

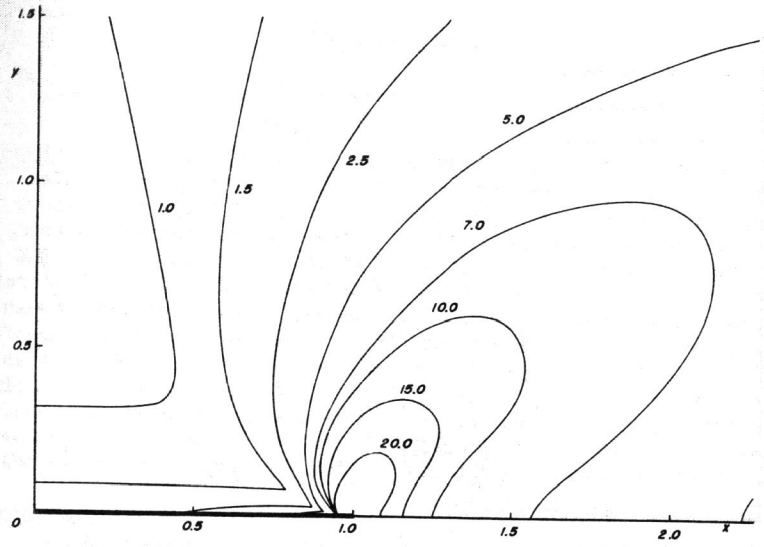

Fig. 11 Contours of $(\epsilon_1 - \epsilon_2) \times 10^3$ at $\bar{\sigma} = 13 \times 10^3$ lb/in^2, reference problem.

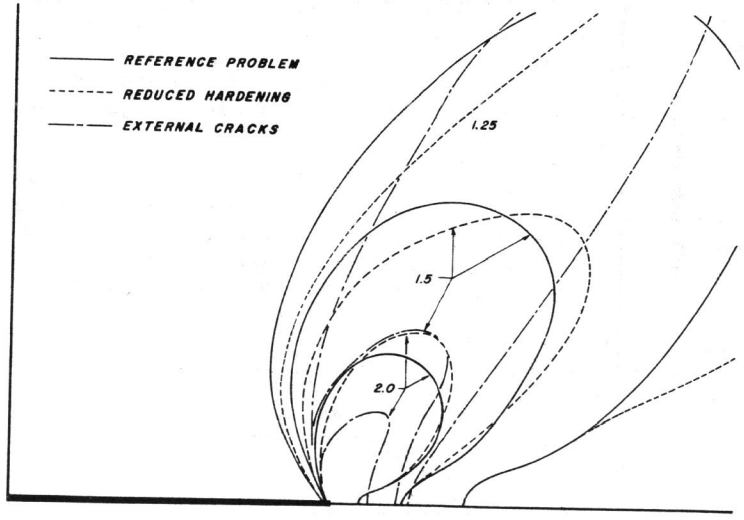

Fig. 12 Contours of $(\epsilon_1 - \epsilon_2) \times 10^3$ at $\bar{\sigma} = 8 \times 10^3$ lb/in^2, three problems.

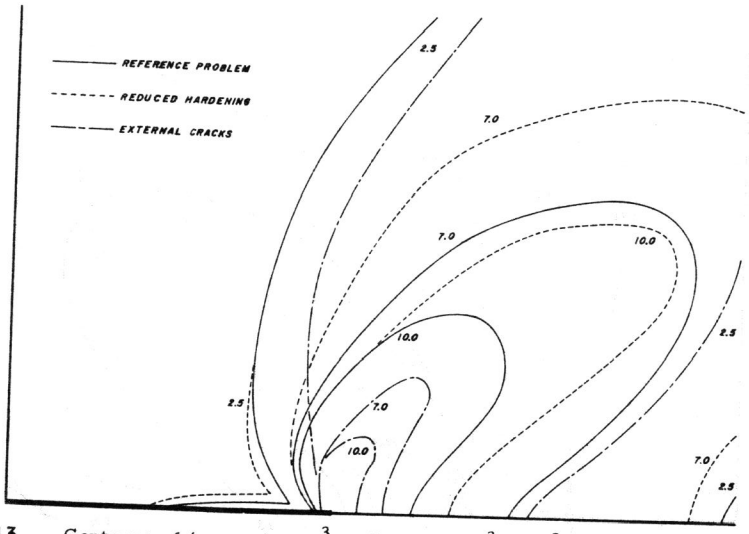

Fig. 13 Contours of $(\epsilon_1 - \epsilon_2) \times 10^3$ at $\bar{\sigma} = 13 \times 10^3$ lb/in^2, three problems.

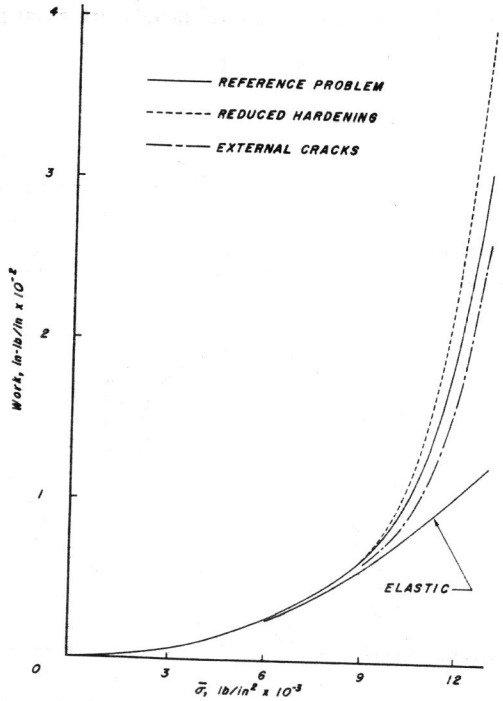

Fig. 14 Variation of work done on one quadrant of the plate, with $\bar{\sigma}$, three problems.

A-17

Plastic Yielding at a Crack Tip

James R. Rice*

Abstract: A model for plastic yielding near a crack tip, based on ideas of Dugdale and Barenblatt, is examined for the case of a through the thickness crack in an elastic plane. General methods of solution for the deformation and stress distributions, accompanying original loading, unloading, and cyclic loading, are given for a class of cracked configurations loaded symmetrically about the crack line. A principal result is that for cases where the size of the zone of plastic deformation is small compared to planar geometric dimensions, stress and deformation near the crack tip are determined solely by the Irwin elastic stress intensity factor for original loading. Similarly, for unloading and cyclic loading, variations in stress and deformation near the crack tip are determined by corresponding variations in the stress intensity factor. Implications of results for the mechanics of fracture and fatigue crack propagation are discussed.

Introduction

The precise determination of the influence of plastic yielding on the deformation and failure at a crack tip is a difficult and presently unresolved problem. Yet such information is needed for accurate predictions of the behavior of cracked bodies under static loads causing fracture and repetitive loads causing fatigue crack propagation. Considerable progress has been made by McClintock [1] and co-workers in the special case of cracked bodies under anti-plane loadings occurring in torsion and longitudinal shear. But predictions in the technically important case of tensile loadings perpendicular to the plane of a crack are presently based, in essence, on an elastic stress analysis or an analogy with elastic-plastic solutions for longitudinal shear. Such an elastic analysis has been used by Irwin [2] and Orowan [3], in extending the classic work by Griffith [4] on fracture of brittle bodies, to develop a criterion of fracture at a crack tip for ductile materials. Paris [5,6] has further used the elastic stress analysis to determine the parameters influencing the rate of propagation of a growing fatigue crack. Aside from more or less empirical corrections to the elastic solution so as to account for plastic yielding, the influence of ductile material behavior has not been taken into consideration.

The role played by plasticity is to some extent clarified by the analysis of a highly simplified model presented here. The model for the influence of plastic yielding, to be described below, will be called the rigid-plastic strip model. The work is motivated by the Barenblatt [7] approach to brittle fracture and by a paper of Dugdale [8] on the yielding of steel

* Assistant Professor of Engineering, Brown University, Providence, R.I., U.S.A.

sheets containing slits. Goodier and Field [9] and the writer, in an unpublished report [10], extended the work of Dugdale by discussing the problems of static fracture and fatigue crack propagation, respectively, through analysis of essentially the same simplified model for the influence of plasticity. The intent of this paper is to extend the analyses of [8,9, and 10] to a wide class of crack problems, to point out the relation of elastic solutions to the elastic-plastic solutions of the strip model, and to discuss implications for the static fracture and fatigue of cracked bodies. Only the case of straight, through-the-thickness cracks in infinite planes loaded so as to induce a state of plane strain or generalized plane stress symmetrical about the crack line is considered. Some relevant results from the elastic solution of crack problems are summarized first.

Elastic Approach to Crack Problems

The elastic solutions to crack problems reveal that stresses are singular at a crack tip. For the type of plane problem considered here it has been shown [11] that the stress σ_y acting (with reference to figure 1) directly ahead of the crack tip ($x=0$) at points along the x axis always has the functional form

$$\sigma_y = K(2\pi x)^{-\frac{1}{2}} + O(x^{\frac{1}{2}}) \,. \qquad (1)$$

Here K is called the "stress intensity factor" and depends on geometric dimensions such as crack length and linearly on the applied loading in a manner which may be determined by a complete solution of the elastic boundary value problem. The expression $O(x^{\frac{1}{2}})$ denotes other non-singular terms in the complete expression for σ_y. Retaining only the singular term of (1), which clearly dominates the elastic stress field near the crack tip, it is seen that the influence of loadings and crack geometry on the elastic stress field near the crack tip is felt solely through the stress intensity factor K.

Thus if plastic yielding occurs only in a small zone near the crack tip and does not seriously redistribute the stresses, the factor K is a single parameter which determines approximately the stress state near the crack tip, and fracture will occur when K reaches a critical value characteristic of the material under consideration. This is the essential result of Irwin's [2] fracture theory; the result is usually obtained through an energy balance approach, expressing the fracture criteria as the achievement of a critical value of the energy release rate [2]

$$\mathcal{G} = \frac{(\eta+1)}{8G} K^2 \,, \qquad (2)$$

where G is the shear modulus and $\eta = 3-4\nu$ for plane strain and $\eta = (3-\nu)/(1+\nu)$ for generalized plane stress, ν being the Poisson ratio. The

fracture criterion based on a critical value of energy release rate is seen, from (2), to be equivalent to the achievement of a critical stress intensity factor. Actually experiment shows [2] that the critical stress intensity factor varies considerably with plate thickness for thin plates. This is presumably due to a transition from a plane strain deformation involving slip in the plane to a plane stress deformation which may involve slip through the thickness, a three dimensional effect which quite naturally is not reflected in the plane elasticity solution. For this reason the critical stress intensity factor is in reality dependent not only on the material under consideration but, for thin plates, also on the plate thickness.

In the case of cyclic loadings, if again the zone of plastic deformation is small and stresses are not seriously redistributed, the history of variation of the stress state near the crack tip depends approximately only on the history of variation of the stress intensity factor K. Thus one expects the rate of fatigue crack propagation to depend on the variation of K, and this is the result found by Paris. Further, it has been experimentally determined [5] that for cyclic loadings the crack growth rate depends primarily on the amplitude of the cyclic variation in K and is relatively insensitive to the mean value of K.

In summary, the results of the elastic analysis are that all problems dealing with the static fracture and fatigue of cracked bodies and involving widely different loadings and geometries are essentially identical problems with the effect of a particular loading and geometry sensed only through the relevant expression for the stress intensity factor, K, provided that plastic yielding does not effect a major redistribution of stress. In what follows, by the analysis of a simple model for the influence of yielding, we shall attempt to see how plastic yielding may modify these results and to what extent the elastic stress intensity factor determines the elastic-plastic solution.

As a preliminary, the Westergaard [12] method of solution is summarized for plane elasticity problems symmetrical about the x axis. Where $F(z)$ is an analytic function of $z = x+iy$, stresses may be expressed as

$$\begin{aligned} \sigma_y &= Re\{F(z)\} + y\, Im\{F'(z)\} \\ \sigma_x &= Re\{F(z)\} - y\, Im\{F'(z)\} \\ \tau_{xy} &= -y\, Re\{F'(z)\} \end{aligned} \qquad (3)$$

For cracks along the x axis $F(z)$ is sectionally holomorphic with a line of discontinuity corresponding to the crack and with an inverse square root singularity at the crack tip. The stress intensity factor is, by comparing (1) and (3), and supposing the crack tip to be at the point

x=c,

$$K = Re\left\{\lim_{z\to c}\left[2\pi(z-c)\right]^{\frac{1}{2}}F(z)\right\} . \qquad (4)$$

The displacement in the y direction is

$$v = \frac{\eta+1}{4G}\,Im\left\{\int_c^z F(z)dz\right\} - \frac{1}{2G}\,y\,Re\left\{F(z)\right\} , \qquad (5)$$

where G is again the shear modulus and η is defined as above in terms of the Poisson ratio through the form appropriate for plane strain or generalized plane stress.

Rigid-Plastic Strip Model

As a first step beyond the purely elastic treatment of crack problems, a model is considered which introduces into the analysis some features of the plastic yielding at the crack tip, but at the same time presents a sufficiently simple mathematical problem so that a complete analysis may be carried out. The model through which it is proposed to simulate the response to loadings of a cracked elastic-plastic plane, as in figure 2 (a), is shown in figure 2(b) and is called the rigid plastic strip model. Through this representation the cracked body becomes two elastic half planes joined together along a strip of rigid-plastic material, with a void in the strip material simulating the crack. The strip is rigid-plastic in the sense that when a y direction normal stress, σ_y, acts on the strip, the material does not extend or contract in the y direction if $|\sigma_y| < \sigma_m$ (where σ_m is the yield stress) but is capable of unlimited deformation if $|\sigma_y| = \sigma_m$. It is assumed that the material offers no resistance to extension or contraction in the x direction. The plastic-strip may be thought of as the plastic analog to well known elastic foundation models.

The strip model is, of course, a rather incomplete abstraction of reality; the zone of plastic deformation has been artificially confined, work hardening has been ignored, no account has been taken of the influence of biaxial and triaxial stress states on the yield condition (although this is not a particularly severe restriction for thin sheets under plane stress), and resistance to extension or contraction in the direction perpendicular to loading has been ignored. Nevertheless, the rigid-plastic strip model does introduce a yielding type behavior into the problem at points ahead of the crack where one knows that plastic relief of high elastic stresses must occur. Further, although the model is clearly incapable of yielding detailed features of the plastic deformation near the crack tip, we may expect a reasonably accurate prediction of gross features such as the plastic zone size, the functional dependence of plasticity effects on external loadings and geometric dimensions, and the behavior

upon unloading and subsequent reloading.

Two general classes of cracked infinite planes symmetrically loaded about the crack line will be considered: 1) bodies sustaining semi-infinite cracks extending from x=0 to x=-∞ where a is the distance of the crack tip from some fixed point, as in figure 3(a), and 2) bodies sustaining a finite crack extending from x=0 to x=-2a for which the loading is also symmetric about a line perpendicular to the crack center, as in figure 4(a). The corresponding rigid-plastic strip models are shown in figures 3(b) and 4(b), where the zone of plastic deformation, ω, has been removed from each strip and stresses of yield strength magnitude σ_m, which the plastic material induces on the elastic half planes, have been drawn over the region ω of plastic deformation. Because of the properties assumed within the rigid plastic strip, the solutions in the elastic regions of the elastic-plastic problems of figures 3(b) and 4(b) are simply the elastic solutions to crack problems where the lengths a are replaced by lengths $a+\omega$, and the yield stress σ_m acting over the distance ω is added to the external loadings.

The problems of figures 3(b) and 4(b) can be solved in general terms, sufficient to cover all possible crack problems of type (1) and (2) above. We assume that the stress intensity factors and Westergaard stress functions of the elastic solution to the crack problems shown in figures 3(a) and 4(a) are known and denote these by $K_e^{(1)}(a)$, $F_e^{(1)}(z,a)$ and $K_e^{(2)}(a)$, $F_e^{(2)}(z,a)$ for the semi-infinite crack and finite crack cases, respectively. Let the solutions to the crack problems defined by yield strength loadings σ_m acting over the distances ω at the crack tips (see figures 5 and 6) be denoted by $K_p^{(1)}(\omega)$, $F_p^{(1)}(z,\omega)$ and $K_p^{(2)}(\omega,a)$, $F_p^{(2)}(z,\omega,a)$ for the semi-infinite and finite cases, respectively. Since one is interested only in superposing solutions, the fact that physical cracks loaded as in figures 5 and 6 would have one side of the crack running into the other is, of course, of no interest.

The size of the plastic zone, ω, is determined by the condition that stresses should be bounded at the outer edges of the plastic zone. This means that the stress intensity factors due to the external loadings (with a replaced by $a+\omega$) and due to the yield strength loadings should sum to zero, and thus ω is the solution of

$$K_e^{(1)}(a+\omega) + K_p^{(1)}(\omega) = 0 \qquad (6\text{-}1)$$

$$K_e^{(2)}(a+\omega) + K_p^{(2)}(\omega,a) = 0 \qquad (6\text{-}2)$$

for the two classes of problems considered. The Westergaard stress functions for the upper elastic half planes of figures 3(b) and 4(b) are obtained by adding the stress functions of the external loadings, with a

replaced by $a+\omega$ and z replaced by $z-\omega$, to the stress functions of the yield strength loadings shown in figures 5 and 6. Thus the complete stress functions for the semi-infinite crack and finite crack cases are

$$F^{(1)}(z) = F_e^{(1)}(z-\omega, a+\omega) + F_p^{(1)}(z,\omega) \tag{7-1}$$

$$F^{(2)}(z) = F_e^{(2)}(z-\omega, a+\omega) + F_p^{(2)}(z,\omega,a), \tag{7-2}$$

respectively, where the ω's are determined by (6-1) and (6-2), respectively. The solution of the rigid-plastic strip model for which K_e and F_e are known functions is thus completed if K_p and F_p are known; expressions for the latter are given below. The Westergaard stress functions $F_p^{(1)}(z,\omega)$ and $F_p^{(2)}(z,\omega,a)$ are obtained by using the solution to concentrated wedging force loads on a crack as a Green's function to generate the solution for distributed loads of intensity σ_m. The algebra is tedious and details will therefore be omitted. The resulting solutions, which may be readily checked by seeing that the boundary conditions of figures 5 and 6 are satisfied (with proper interpretation of branch cuts), are

$$F_p^{(1)}(z,\omega) = -\frac{2\sigma_m}{\pi}\left[\left(\frac{\omega}{z-\omega}\right)^{1/2} - \tan^{-1}\left(\frac{\omega}{z-\omega}\right)^{1/2}\right] \tag{8-1}$$

$$F_p^{(2)}(z,\omega,a) = -\sigma_m\left(1-\frac{2}{\pi}\sin^{-1}\left(\frac{a}{a+\omega}\right)\right)\frac{z+a}{[(z+a)^2-(a+\omega)^2]^{1/2}} \tag{8-2}$$

$$+\sigma_m\left\{1-\frac{2}{\pi}\tan^{-1}\left[\frac{a}{z+a}\left(\frac{(z+a)^2-(a+\omega)^2}{(a+\omega)^2-a^2}\right)^{1/2}\right]\right\}$$

The corresponding stress intensity factors for the two classes of problems under consideration are, by an application of (4),

$$K_p^{(1)}(\omega) = -2\sqrt{\frac{2}{\pi}}\,\sigma_m\sqrt{\omega} \tag{9-1}$$

$$K_p^{(2)}(\omega,a) = -\sigma_m\sqrt{\pi(a+\omega)}\left(1-\frac{2}{\pi}\sin^{-1}\left(\frac{a}{a+\omega}\right)\right). \tag{9-2}$$

Equations (6-1) and (6-2) for the size of the plastic zone, ω, become

$$2\sqrt{\frac{2}{\pi}}\,\sigma_m\sqrt{\omega} = K_e^{(1)}(a+\omega) \tag{10-1}$$

$$\sigma_m\sqrt{\pi(a+\omega)}\left(1-\frac{2}{\pi}\sin^{-1}\left(\frac{a}{a+\omega}\right)\right) = K_e^{(2)}(a+\omega). \tag{10-2}$$

An important result follows by rearranging the above two equations in the form

$$\omega = \frac{\pi}{8\sigma_m^2}\left[K_e^{(1)}(a+\omega)\right]^2 \tag{11-1}$$

$$\omega = a\left\{\sec\left[\frac{\sqrt{\pi}}{2}\,\frac{K_e^{(2)}(a+\omega)}{\sigma_m\sqrt{a+\omega}}\right]-1\right\}$$

$$= a + \frac{\pi}{8\sigma_m^2}\left[K_e^{(2)}(a+\omega)\right]^2\left(\frac{a}{a+\omega}\right) + \cdots - a \tag{11-2}$$

Assuming ω to be a negligible fraction of a and neglecting all terms of order ω/a in comparison to unity, one has $K_e(a+\omega) \approx K_e(a) \equiv K_e$, and both (11-1) and (11-2) result in

$$\omega \approx \frac{K_e^2}{8\sigma_m^2} \tag{12}$$

Thus when the scale of plasticity is small ($\omega \ll a$), it is seen that for all crack problems, irrespective of the manner of loading, the plastic zone size depends on the loading and geometry only through the elastic stress intensity factor K_e. By considering some specific loadings in the next section it will be seen further that the entire stress and displacement field near the crack tip depends also on the loadings and geometry only through the stress intensity factor K_e in the case of small scale plasticity, although a more complicated dependence is indicated when ω is a substantial fraction of a.

Equation (12) and subsequent small scale yielding equations are derived from stress fields for cracks in infinite planes. However, it is easily seen that all expressions given for small scale yielding are also valid for cracks in finite planes, provided that the plastic zone size is negligible not only in comparison to crack length but also in comparison to all planar dimensions of the cracked body. When this condition is met, the computations of (8-1) and (9-1), for effects of the yield stresses restraining the crack surfaces near its tip, are valid and the effects of finite specimen dimensions are sensed only through the relevant expression for the elastic stress intensity factor, K_e, appearing in (12).

A measure of the plastic deformation near the crack may be obtained by solving for the y direction displacement, $v(x)$, of the rigid-plastic strip material at points along the x axis. Noting that there is zero displacement at $x = \omega$, equation (5) results in

$$v(x) = \frac{\eta+1}{4G} I_m\left\{\int_{\omega}^{x} F(z)\,dz\right\} \qquad (13)$$

In the sequel displacement results are given in a form valid for either plane strain or plane stress. However, the strip model is clearly more appropriate under plane stress conditions where yielding takes place on planes inclined at 45° with the x-y plane and a maximum tensile stress yield condition governs.

Solutions to Particular Problems

The results of the analysis are further clarified by considering in detail some particular problems representative of different types of crack loadings which arise in practice. Two problems, each representing a particular case of the two general classes considered in the last section, are stated below and solved by the general methods of the last section:

1) An infinite plane with a semi-infinite crack opened by concentrated forces P per unit thickness at a distance a from the crack tip, as shown in figure 7.

2) An infinite plane with a finite crack of length 2a opened by a uniform tensile stress σ at infinity, as shown in figure 8.

As may easily be verified, the Westergaard stress functions and, from (), the corresponding stress intensity factors, of the elastic solutions the above problems are

$$F_e^{(1)}(z,a) = \frac{P}{\pi(z+a)}\left(\frac{a}{z}\right)^{1/2}, \quad K_e^{(1)}(a) = \frac{\sqrt{2}\,P}{\sqrt{\pi a}} \qquad (14\text{-}1)$$

$$F_e^{(2)}(z,a) = \frac{\sigma(z+a)}{[(z+a)^2-a^2]^{1/2}}, \quad K_e^{(2)}(a) = \sigma\sqrt{\pi a} \qquad (14\text{-}2)$$

Actually, a uniform compressive stress $\sigma_x = -\sigma$ must be added to the stress function of (14-2) to satisfy the boundary conditions of figure 8. Since such a stress field has no influence on the stress intensity factor (in the strip model solution, it will be subsequently ignored.) The plastic zone sizes are obtained by inserting the expressions for K_e above into equations (10), using (10-1) for problem 1, and (10-2) for problem 2.

The resulting expressions for the respective plastic zone sizes are

$$\omega = \frac{a}{2}\left[\left(1+\frac{P^2}{a^2\sigma_m^2}\right)^{1/2} - 1\right] \qquad (15\text{-}1)$$

$$\omega = a\left[\sec\left(\frac{\pi}{2}\frac{\sigma}{\sigma_m}\right) - 1\right] \qquad (15\text{-}2)$$

The complete stress functions for the plastic strip model are found through inserting the elastic stress functions, F_e, of equations (14) into the formalism of equations (7), where the functions $F_p^{(1)}(z,\omega)$ and $F_p^{(2)}(z,\omega,a)$ occurring in (7) are given by (8). It is convenient to repress explicit dependence on the external loadings P and σ by writing the loads as functions of plastic zone size, ω, through an inversion of equations (15-1 and 2) respectively. There results, after some manipulations,

$$F^{(1)}(z) = \frac{2\sigma_m}{\pi}\left\{\tan^{-1}\left(\frac{\omega}{z-\omega}\right)^{1/2} - \frac{[\omega(z-\omega)]^{1/2}}{a+z}\right\} \qquad (16\text{-}1)$$

$$F^{(2)}(z) = \frac{2\sigma_m}{\pi}\tan^{-1}\left[\left(\frac{\omega}{z-\omega}\right)^{1/2}\left(\frac{2a+\omega}{z+2a+\omega}\right)^{1/2}\frac{z+a}{a}\right] \qquad (16\text{-}2)$$

for problems 1 and 2 respectively, where the value of ω for each problem is given in terms of the relevant loading, P or σ, by equations (15).

If one considers values of z of the order of ω (that is, confine attention to points near the crack tip) and supposes that ω is a negligible fraction of a, the last term in (16-1) is negligible and the factor of $\left(\frac{\omega}{z-\omega}\right)^{\frac{1}{2}}$ in (16-2) differs from unity by a negligible amount. Thus in the case of small scale plasticity both $F^{(1)}(z)$ and $F^{(2)}(z)$ become, for points near the crack tip,

$$F(z) = \frac{2\sigma_m}{\pi}\tan^{-1}\left(\frac{\omega}{z-\omega}\right)^{1/2}, \qquad (17)$$

which shows that the two problems treated here, involving different loadings and geometry, have stress and displacement fields near the crack tip which are functionally identical when $\omega \ll a$. Recalling (12)

$$\omega = \frac{\pi K_e^2}{8\sigma_m^2} \tag{12}$$

appropriate when $\omega \ll a$, (this may be readily verified independently (12) for the two particular problems presently under consideration by panding equations (15) as a Taylor series in the applied loadings, taining the first non-zero term, and comparing with the stress in- nsity factors as given by equations (14)), and it is seen that in the se of small scale plastic yielding the crack tip stress and displacement elds depend on external loadings and geometry only through the elastic ress intensity factor K_e. When ω is a substantial fraction of a the ve remarks are, of course, no longer valid and quantitative estimates the influence of plasticity may be had through application of equations) for the plastic zone size and (16) for the stress functions.

The displacements of the rigid-plastic strip give a measure of the stic deformation and may be calculated from (13). The results, valid $0 < x < \omega$, are, for the two problems

$$v^{(1)}(x) = \frac{(\eta+1)\sigma_m\omega}{2\pi G}\left\{(1-\frac{x}{\omega})^{1/2} - \frac{1}{2}\frac{x}{\omega}\log\left(\frac{1+(1-x/\omega)^{1/2}}{1-(1-x/\omega)^{1/2}}\right)\right.$$
$$\left. + \log\left(\frac{(1+a/\omega)^{1/2}+(1-x/\omega)^{1/2}}{(1+a/\omega)^{1/2}-(1-x/\omega)^{1/2}}\right)\right\} \tag{18-1}$$

$$v^{(2)}(x) = \frac{(\eta+1)\sigma_m a}{4\pi G}\left\{\log\left[\frac{1+\left(\frac{2a+\omega+x}{2a+\omega}\right)^{1/2}(1-x/\omega)^{1/2}}{1-\left(\frac{2a+\omega+x}{2a+\omega}\right)^{1/2}(1-x/\omega)^{1/2}}\right]\right.$$
$$\left. - \left(1+\frac{x}{a}\right)\log\left[\frac{1+x/a\left(\frac{2a+\omega+x}{2a+\omega}\right)^{1/2}(1-x/\omega)^{1/2}}{1+x/a-\left(\frac{2a+\omega+x}{2a+\omega}\right)^{1/2}(1-x/\omega)^{1/2}}\right]\right\} \tag{18-2}$$

esponding maximum rigid-plastic strip displacements, v_o, occurring at crack tip x=0, are obtained from (18-1) and (18-2) after an applica- of L'Hopital's rule, yielding

$$v_o^{(1)} = \frac{(\eta+1)\sigma_m\omega}{2\pi G}\left\{1+2\log\left[(1+\frac{\omega}{a})^{1/2}+(\frac{\omega}{a})^{1/2}\right]\right\} \tag{19-1}$$

$$v_o^{(2)} = \frac{(\eta+1)\sigma_m\omega}{2\pi G}\left\{\frac{2}{\omega}\log(1+\frac{\omega}{2})\right\} \tag{19-2}$$

for the semi-infinite crack under wedge forces and finite crack with stresses at infinity, respectively.

The expressions for displacements in the case of small scale yielding may be obtained directly from $F(z)$ of equation (17) which has been shown to be the limit of $F^{(1)}(z)$ and $F^{(2)}(a)$ when $\omega \ll a$. Upon application of (13) one obtains strip displacements

$$v(x) = \frac{(\eta+1)\sigma_m\omega}{2\pi G}\left\{(1-x/\omega)^{1/2} - \frac{1}{2}\frac{x}{\omega}\log\left[\frac{1+(1-x/\omega)^{1/2}}{1-(1-x/\omega)^{1/2}}\right]\right\} \tag{20}$$

for the limit of $v^{(1)}(x)$ and $v^{(2)}(x)$, and maximum displacement at the crack tip

$$v_o = \frac{(\eta+1)\sigma_m\omega}{2\pi G} = \frac{(\eta+1)K_e^2}{16G\sigma_m} \tag{21}$$

for the limit of $v_o^{(1)}$ and $v_o^{(2)}$, where (12), appropriate when $\omega \ll a$, has been used. Equations (20) and (21) may, of course, be obtained directly from (18-1,2) and (19-1,2) by neglecting all terms of order ω/a.

The results of the detailed solutions given in this section will be used later in a discussion of static fracture and fatigue. The solution of other crack problems involving different loadings and geometries may also be obtained in analogy to the methods of this section and the last. Of particular interest from the point of view of practical applications would be solutions of the rigid-plastic strip model for configurations such as a central crack in a finite plane body and an edge crack extending into a plane body from a free surface. Since the methods involved in the analysis of the strip model are essentially the same methods used in the conventional elastic treatment of crack problems (in fact, the entire plastic strip analysis may be carried out once the elastic Green's function for wedging forces on the crack surface is known), methods of solution as in [13-16] might be of use for such problems.

Unloading and Repeated Loadings

When the load on a cracked body is decreased one expects the yielded material near the crack tip to be forced back toward its original position and thus yield in compression. This phenomena is investigated here through the rigid-plastic strip model. The analysis is surprisingly

simple, for in solving the original loading problem most of the work has already been done. To formulate the unloading problem in general terms, suppose a cracked body is subjected to a set of external loads proportional to some loading parameter L, and that a is some geometric dimension indicating crack length. Then in solving the original loading problem a relation has been determined of the type (15) giving the plastic zone size as a function of load, yield stress, and crack length in the form

$$\omega = \Omega(L, \sigma_m, a) \ . \tag{22}$$

The Westergaard stress function for the elastic region above the strip has the form (where, as in deriving (16), dependence on the load L is converted to dependence of ω through inverting (22))

$$F(z) = \mathcal{F}(z, \omega, a, \sigma_m) \ , \tag{23}$$

and strip displacements may be written in the form, analagous to (18),

$$V(x) = V(x, \omega, a, \sigma_m) \ , \quad 0 < x < \omega \ . \tag{24}$$

Now suppose the load is decreased by an amount ΔL to $L-\Delta L$. A part of the original plastic zone goes into compressive yielding; we shall suppose this zone to have length ω' and call it the zone of reversed plastic deformation. With reference to figure 9 where only the upper half plane is shown, the elastic solution which must be added to the original elastic solution is one in which the crack is pushed shut with a load ΔL and in which this closing is opposed by a stress $2\sigma_m$ acting over a distance ω' in front of the crack, the additional strip displacement being zero elsewhere. Clearly ω' is chosen such that that total stress intensity factor at $x=\omega'$ due to load ΔL and the boundary stress $2\sigma_m$ sums to zero. Thus the additional elastic solution is functionally identical to the original elastic solution except that L is replaced by $-\Delta L$, σ_m is replaced by $-2\sigma_m$, and ω is replaced by ω'. The reversed plastic zone is, therefore, from (22)

$$\omega' = \Omega(-\Delta L, -2\sigma_m, a) \ . \tag{25}$$

The stress function and displacement after unloading are obtained by adding to the original expressions (23) and (24) the expressions due to the added stresses shown in the center of figure 9, the latter expressions being obtained from (23) and (24) after making the substitutions indicated above. Thus, after unloading,

$$F(z) = \mathcal{F}(z, \omega, a, \sigma_m) + \mathcal{F}(z, \omega', a, -2\sigma_m) \ , \tag{26}$$

and

$$V(x) = \begin{cases} V(x, \omega, a, \sigma_m) + V(x, \omega', a, -2\sigma_m) \ , & 0 < x < \omega' \\ V(x, \omega, a, \sigma_m) \ , & \omega' < x < \omega \ . \end{cases} \tag{27}$$

Details of the unloading solution may be readily obtained for the two specific problems treated in the last section through the formalism of equations (25-27). For the case of wedge forces per unit thickness P opening a semi-infinite crack and of tensile stresses σ opening a finite crack, suppose the loads are decreased by amounts ΔP and $\Delta\sigma$, respectively. Then through use of equation (25) and equations (15), the sizes ω' of the zones of reversed plastic deformation are

$$\omega' = \frac{a}{2}\left[\left(1 + \frac{(\Delta P)^2}{4a^2\sigma_m^2}\right)^{1/2} - 1\right] \tag{28-1}$$

$$\omega' = a\left[\sec\left(\frac{\pi(\Delta\sigma)}{4\sigma_m}\right) - 1\right] \tag{28-2}$$

respectively. By evaluating (27) at x=0 and through use of equations (19), the final crack tip displacements in the two cases after unloading are given by

$$V_o^{(1)} = \frac{(\eta+1)\sigma_m}{2\pi G}\left\{(\omega - 2\omega')\log\left(\left(1+\frac{\omega}{a}\right)^{1/2} + \left(\frac{\omega}{a}\right)^{1/2}\right] - 4\omega'\log\left(\left(1+\frac{\omega'}{a}\right)^{1/2} + \left(\frac{\omega'}{a}\right)^{1/2}\right]\right\} \tag{29-1}$$

$$V_o^{(2)} = \frac{(\eta+1)\sigma_m a}{2\pi G}\left\{\log\left(1+\frac{\omega}{a}\right) - 2\log\left(1+\frac{\omega'}{a}\right)\right\} , \tag{29-2}$$

respectively. Results for the complete stress and displacement functions after unloading may be filled in through use of (26) and (27) in conjunction with (16) and (18). These lead to lengthy and unrevealing expressions which will not be recorded here. Instead, the complete unloading solution will be given in the case of small scale plastic yielding ($\omega', \omega \ll a$), a case in which it has been shown that the stress

and displacement fields are functionally identical for all problems and that the influence of loads and geometry is sensed only through the elastic stress intensity factor, K_e. Instead of proceeding to this case as a limit of the two unloading solutions considered above, the limiting loading solutions already derived for the case of small scale yielding will be used directly.

Suppose that the cracked body is loaded so that the elastic stress intensity factor is K_e. Then ω (here assumed $\ll a$) is given by (12), the stress function by (17), and displacements by (20), which are the special forms of (22), (23), and (24) appropriate in the present case. Now suppose the loads are decreased so that the stress intensity factor decreases by ΔK_e. Then the zone of reversed plastic deformation ω', is by (25)

$$\omega' = \frac{\pi}{32}\frac{(\Delta K_e)^2}{\sigma_m^2}, \quad \left(\text{recall } \omega = \frac{\pi}{8}\frac{K_e^2}{\sigma_m^2}\right). \tag{30}$$

Equation (26) for the stress function after unloading becomes

$$F(z) = \frac{2\sigma_m}{\pi}\left\{\tan^{-1}\left(\frac{\omega}{\omega - z}\right)^{1/2} - 2\tan^{-1}\left(\frac{\omega'}{\omega' - z}\right)^{1/2}\right\}, \tag{31}$$

and the final displacements of the material in the reversed zone are, by (27),

$$v(x) = \frac{(\eta+1)\sigma_m}{2\pi G}\left\{\omega(1-x/\omega)^{1/2} - 2\omega'(1-x/\omega')^{1/2}\right.$$
$$\left. - \tfrac{1}{2}x\log\left[\frac{1+(1-x/\omega)^{1/2}}{1-(1-x/\omega)^{1/2}}\right] + x\log\left[\frac{1+(1-x/\omega')^{1/2}}{1-(1-x/\omega')^{1/2}}\right]\right\} \tag{32}$$
$$0 < x < \omega'.$$

The final displacement at the crack tip $x = 0$ is

$$v_0 = \frac{(\eta+1)\sigma_m}{2\pi G}(\omega - 2\omega') = \frac{(\eta+1)}{16 G\sigma_m}\left[K_e^2 - \tfrac{1}{2}(\Delta K_e)^2\right], \tag{33}$$

where (30) has been used.

If the cracked body is completely unloaded so that $\Delta K_e = K_e$, the reversed plastic zone (30) is seen to be one-quarter of the original

plastic zone and the strip displacement (33) at the crack tip is seen to be one-half of the displacement before removal of the load. Equations (28, 29, 30, and 33) further indicate that the reversed plastic zone and change in plastic deformation depend only on the decrease in load, being independent of the original load level. If unloading is followed by a reloading which brings the load back to its original level, it is easily shown that the solution is identical to the solution before unloading. Thus during a cyclic loading the model predicts a cyclic deformation in the reversed plastic zone dependent only on the amplitude of load fluctuation and independent of the mean load.

Remarks above have some relevance to experimental studies of plastic deformation near a crack tip such as [17,18], where cracked specimens are studied after unloading, as the present results indicate that unloading markedly alters the state of stress and deformation. Further, it appears that an unloading solution given in [17] for the finite crack in a tensile field is incorrect, leading to results at variance with (28-2) and (29-2).

Comparison With an Exact Solution

Some idea of the adequacy of the rigid-plastic strip model may be obtained by comparison with an exact elastic-plastic solution. Such is available from the work of McClintock [1] for the case of longitudinal shear in which the deformation consists of warping displacements only in the z direction (perpendicular to the crack x,y plane), and the only non-zero stresses are the shears τ_{xz}, τ_{yz}. Such anti-plane problems are solved by an analytic function $H(z)$ where shear stresses and warping displacements are given in elastic material by

$$\tau_{yz} + i\tau_{xz} = H(z)$$
$$w = \frac{1}{G} I_m\left\{\int H(z)\,dz\right\} \tag{34}$$

Consider a semi-infinite crack along the negative x axis with tip at the origin, and for which the elastic solution is

$$H(z) = K_w(2\pi z)^{-1/2} \tag{35}$$

where K_w is the stress intensity factor for warping displacements. The exact elastic-plastic solution of this problem has a circular yield zone of diameter ω with center at $x = \omega/2$. Where τ_m is the yield stress, the solution is

$$\tau_{rz} = 0, \quad \tau_{\theta z} = \tau_m \text{ in plastic zone } \left|z - \frac{\omega}{2}\right| < \frac{\omega}{2} \tag{36}$$

$$H(z) = \tau_m \sqrt{\frac{\omega}{2}} \left(z - \frac{\omega}{2}\right)^{-\frac{1}{2}} \quad \text{in elastic zone } \left|z - \frac{\omega}{2}\right| > \frac{\omega}{2}$$

with

$$\omega = \frac{1}{\pi} \frac{K_w^2}{\tau_m^2} \ . \tag{37}$$

Postulating a rigid-plastic strip model for this case, the solution may be shown to be

$$H(z) = \frac{2\tau_m}{\pi} \tan^{-1}\left(\frac{\omega}{z-\omega}\right)^{1/2} , \tag{38}$$

with

$$\omega = \frac{\pi}{8} \frac{K_w^2}{\tau_m^2} \ . \tag{39}$$

Solving for the maximum displacement w_o at the crack tip from (34), for the exact solution (the displacement field actually has a discontinuous jump of $2w_o$ at the crack tip in the exact solution!)

$$w_o = \frac{1}{G} \tau_m \omega = \frac{1}{\pi} \frac{K_w^2}{G\tau_m} \ , \tag{40}$$

and for the solution of the rigid-plastic strip model

$$w_o = \frac{2}{\pi G} \tau_m \omega = \frac{1}{4} \frac{K_w^2}{G\tau_m} \ . \tag{41}$$

Comparing (37) with (39) and (40) with (41), it is seen that the rigid-plastic strip model predicts a plastic zone about 20% too large and a maximum crack tip displacement about 25% too small. The relatively close agreement between the exact solution and the results of a plastic strip analysis suggests that artifically confining the zone of plastic deformation (by requiring, in the model, that plastic effects take place only in the rigid-plastic strip of material ahead of the crack) does not introduce an appreciable error in the prediction of gross features of the deformation, such as, for example, the plastic zone size and tip displacement. This accuracy of the strip model is further clarified by the longitudinal shear solution of [19], and by the experimental results of

Dugdale [8] and Hahn and Rosenfield (17) in tests of plates with slits under tensile loadings.

Fracture and Fatigue

The strip model does not yield enough information on the details of plastic yielding to permit the absolute prediction of fracture strengths of cracked bodies in terms of material constants and geometric dimensions. However, the model may be utilized in a semi-empirical method to predict fracture criteria from a limited amount of experimental data. The solutions presented earlier for plastic zone size (12), stress function (17), and strip displacements (20,21) indicate that when the plastic zone size, ω, is negligible compared to crack length, a, the stress and deformation near the crack tip depend on applied loadings and the geometric configuration only through the elastic stress intensity factor, K_e. Thus, in the case of small scale yielding, one expects fracture to occur when K_e reaches a critical value in agreement with the Griffith-Irwin criteria. Let K_e^f be this critical stress intensity factor at fracture, as obtained from some experiment on a cracked body for which the plastic zone size at fracture is negligible in comparison to geometric dimensions. The corresponding plastic zone size, ω_f, is from (12)

$$\omega_f = \frac{\pi}{8} \frac{(K_e^f)^2}{\sigma_m^2} \tag{42}$$

and crack tip displacement, v_o^f, is from (21)

$$v_o^f = \frac{(\eta+1)\sigma_m}{2\pi G} \omega_f \ . \tag{43}$$

For subsequent work it will be convenient to view ω_f, the plastic zone size at failure in a small scale yielding fracture experiment, as a characteristic length defined by (42) for a given material, temperature of test, and plate thickness. It will be seen, then, that fracture criteria depend on the ratio of crack length to this characteristic length.

The choice of a fracture criteria when yielding is not on a small scale is somewhat arbitrary in the absence of detailed features of the plastic deformation. However, it is clear that a criterion should be based on parameters describing local behavior in the immediate vicinity of the crack tip where fracture initiates. It is then reasonable to assume fracture occurs when the maximum strip displacement, v_o, at the crack tip reaches a critical value, v_o^f, as given by (43), since v_o gives

a measure of the deformation near the crack tip and may be expected to reflect the influence of applied loadings and geometry in an essentially correct way. Fracture criteria are derived below by setting $v_o = v_o^f$ for the cases treated earlier of wedge forces per unit thickness P opening a semi-infinite crack at distance a from the tip and of tensile stresses σ opening a finite crack of length 2a. Equating (19-1) and (19-2) to (43) and cancelling the common coefficient, one obtains

$$\omega_f = \omega\left\{1 + 2\log\left((1+\frac{\omega}{a})^{1/2} + (\frac{\omega}{a})^{1/2}\right)\right\} \tag{44-1}$$

$$\omega_f = a\log\left(1+\frac{\omega}{a}\right), \tag{44-2}$$

respectively, for the two cases. Using equations (15) to express dependence on the applied loadings, after some rearrangement equations (44) yield for the respective fracture loads P_f and σ_f

$$\frac{\omega_f}{a} = \frac{1}{2}\left\{\left(1+\left(\frac{\omega_f}{a}\right)^2\left(\frac{P_f}{\sigma_m\omega_f}\right)^2\right)^{1/2} - 1\right\} - \log\left\{\left(\frac{\omega_f}{a}\right)\left(\frac{P_f}{\sigma_m\omega_f}\right) + \left(1+\left(\frac{\omega_f}{a}\right)^2\left(\frac{P_f}{\sigma_m\omega_f}\right)^2\right)^{1/2}\right\}. \tag{45-1}$$

$$\frac{\sigma_f}{\sigma_m} = \frac{2}{\pi}\cos^{-1}\left(\exp\left(-\frac{\omega_f}{a}\right)\right) \tag{45-2}$$

Equation (45-1) may not be solved explicitly but gives an implicit relation between the dimensionless wedge loading at fracture, $\frac{P_f}{\sigma_m\omega_f}$, and the dimensionless crack length, $\frac{a}{\omega_f}$.

The Griffith-Irwin fracture theory predicts failure when the elastic stress intensity factor reaches the critical value K_e^f. Taking the appropriate expressions for K_e from (14), this criterion becomes

$$\frac{\sqrt{2}\,P_f}{\sqrt{\pi a}} = K_e^f \tag{46-1}$$

$$\sigma_f\sqrt{\pi a} = K_e^f \tag{46-2}$$

Comparison with (45) is facilitated by replacing K_e^f through (42) which defines ω_f. There results

$$\frac{P_f}{\sigma_m\omega_f} = 2\sqrt{\frac{a}{\omega_f}} \tag{47-1}$$

$$\frac{\sigma_f}{\sigma_m} = \frac{2\sqrt{2}}{\pi}\sqrt{\frac{\omega_f}{a}} \tag{47-2}$$

for the corresponding Griffith-Irwin fracture criteria.

A comparison of the variation of fracture stress, σ_f, with half crack length, a, as predicted by the rigid-plastic strip model (45-2) and by the Griffith-Irwin criteria (47-2) is made in figure 10, which clearly points out the agreement between the two criteria for small scale yielding ($\omega_f \ll a$). Numerical calculations indicated that the Griffith-Irwin fracture stress exceeded the strip model fracture stress by 1% when $a = 20\omega_f$, 5% when $a = 3.7\omega_f$, 10% when $a = 1.8\omega_f$, 20% when $a = 0.9\omega_f$, and 40% when $a = 0.5\omega_f$. It is noted that the strip model predicts fracture at $\sigma = \sigma_m$ as $a \to 0$ which corresponds to yielding of the entire rigid-plastic strip.

Fracture criteria given here may be expected to be reliable under plane stress conditions for which the yield condition is a realistic one and experimental evidence [8,17] confirms the ability of the model in predicting gross features of the yielding behavior. It is noted that the solutions presented for the strip model are independent of the strip thickness in the y direction. Indications from [17] are that by identifying this height with plate thickness t so that the average plastic strain is $2v_o/t$ and supposing fracture to occur when this average strain reaches a value characteristic of fracture in a tensile test, plane stress fracture strengths and their variation with plate thickness may be predicted with reasonable accuracy.

Failure criteria similar to equations (45) may be obtained for other crack configurations by solving for the crack tip displacement, v_o, of the corresponding rigid-plastic strip model and equating it to v_o^f of (43). Of particular interest would be fracture criteria for edge cracks, cracks

in finite sheets, and cracks emanating from cut-outs. Generalizations of the strip model may also lead to useful results. Essentially, the model allows the type of non-elastic material behavior of interest at the crack tip (in the present case, plastic yielding) to occur in a small artificially confined zone (the strip) ahead of the tip. Mathematical complexities are reduced since the non-elastic behavior enters the analysis only through boundary conditions imposed on the elastic regions bounding the strip, in which such behaviors as workhardening and strain rate sensitivity may be allowed.

Solutions of the strip model for unloading and repetitive loadings have implications for fatigue crack propagation. The general solution of (25) and (27) for unloading indicates that the zone of reversed plastic yielding and change in strip deformation depend only on the decrement in applied load, and not on the load level before unloading. Thus, under a cyclic loading, the strip model predicts a cyclic plastic deformation near the crack tip which depends only on the amplitude of load fluctuation and not on the mean level about which the load is cycled. Associating the growth of a fatigue crack with this cyclic deformation, one expects the crack propagation rate to depend primarily on the amplitude of load fluctuation and to be comparatively insensitive to the mean load level. This conclusion is supported by experimental results cited in [5,6] and other references therein.

When the zone of reversed deformation is small compared to crack length ($\omega \ll a$) the unloading solutions of (30), (32), and (33) are valid, and it is seen that the cyclic plastic deformation under a fatigue loading depends only on the amplitude of variation, ΔK_e, in the elastic stress intensity factor. Thus, for small scale reverse yielding, the model suggests that crack propagation rates depend on the geometrical configuration of the cracked body and fluctuations in applied loadings only through the variation in the elastic stress intensity factor. This is the conclusion reached by Paris [5,6] and verified experimentally by a wide range of data, from several investigators, for different metals and different cyclic loading conditions, including in [6] some data obtained under random loadings. A fatigue crack growth law in which the crack extension per load cycle is proportional to $(\Delta K_e)^4$ is derived in [10] from the unloading solution for the strip model under the assumption that failure by fatigue occurs at a material point ahead of the crack when the total of plastic deformations at that point (as measured by the sum of absolute values of the reversing strip displacements) reaches a critical value. This is in agreement with the power law proposed in [5] as the best fit to the entire range of available data on crack propagation. Corrections for cases where the scale of reverse yielding is not small may be made by using equations such as (28) and (29) to describe the cyclic deformation, in lieu of the small scale yielding equations (30) and (33).

Certain important aspects (in addition to three dimensional effects) of

the fracture and fatigue of cracked bodies, while presumably due to plastic yielding at a crack tip, seem not to be predictable through an analysis of the strip model. One of these is the phenomena of slow growth [20], whereby catastrophic fracture does not occur all at once, but rather the crack grows gradually after a certain load level is exceeded until, under increasing load, a critical point is reached at which catastrophic fracture ensues. An explanation proposed in [20], notes that plastic materials have history sensitive deformation laws, implying that the distribution of plastic yielding due to stressing the tip region of a stationary crack by increasing applied loadings is different from the distribution of yielding caused by extending the crack under stationary applied loads. Such a distinction does not occur in the strip model. Another phenomena is the delay effect [21] which occurs in the course of fatigue crack propagation under cyclic loading when a very large overload is applied; the result of the overload is to effectively stop the crack growth for a large number of load cycles. Presumably, an elastic "shakedown" occurs through severe blunting of the crack tip by large plastic deformations of the overload. The strip model, on the other hand, predicts no change in the pattern of reversing plastic deformation.

Acknowledgement

Work reported here was initiated at Lehigh University through financial support of a National Science Foundation graduate fellowship, and completed at Brown University through support of a National Academy of Sciences-National Research Council postdoctoral fellowship funded by the Air Force Office of Scientific Research. Financial assistance in the preparation of the manuscript was provided by the Advanced Research Projects Agency. The author gratefully acknowledges this financial support, and expresses gratitude to Dr. P. C. Paris of Lehigh University for helpful discussions of the work.

References

1) F. A. McClintock, "On the Plasticity of the Growth of Fatigue Cracks", in Fracture of Solids, (eds. D.C. Drucker and J.J. Gilman), Wiley, 1963.

2) G. R. Irwin, "Fracture Mechanics", in Structural Mechanics, Pergamon Press, 1960.

3) E. Orowan, "Energy Criteria of Fracture", Weld. J. Res. Suppl., March, 1955.

4) A. A. Griffith, "The Phenomena of Flow and Rupture in Solids", Phil. Trans., Roy. Soc. London, A221, 163, 1921.

5) P. C. Paris and F. Erdogan, "A Critical Analysis of Crack Propagation Laws", J. Basic Engrg., vol.85, 4, Dec. 1963.

6) P. C. Paris, "The Fracture Mechanics Approach to Fatigue", in Fatigue-An Interdisciplinary Approach, (eds. Weiss et al.), Syracuse Univ. Press, 1964.

7) G. I. Barenblatt, "On Equilibrium Cracks Formed in Brittle Fracture", Appl. Math. Mech., vol. 23, 3, 1959.

8) D. S. Dugdale, "Yielding of Steel Sheets Containing Slits", J. Mech. Phys. Solids, vol. 8, 1960.

9) J. N. Goodier and F. A. Field, "Plastic Energy Dissipation in Crack Propagation", in Fracture of Solids, (eds. D.C. Drucker and J.J. Gilman), Wiley, 1963.

10) J. R. Rice, "Fatigue Crack Growth Model: Some General Comments and Preliminary Study of the Rigid Plastic Strip Model", (unpublished) Lehigh Univ. Institute of Research Report, Dec. 1962.

11) M. L. Williams, "On the Stress Distribution at the Base of a Stationary Crack", J. Appl. Mech., vol. 24, 1, March 1957.

12) H. M. Westergaard, "Bearing Pressure on Cracks", J. Appl. Mech., vol. 6, June 1939.

13) O. L. Bowie, "Rectangular Tensile Sheet With Symmetric Edge Cracks", J. Appl. Mech., vol. 31, 2, June 1964.

14) A. S. Kobayashi, R. B. Cherepy, and W. C. Kinsel, "A Numerical Procedure for Estimating the Stress Intensity Factor of a Crack in a Finite Plate", J. Basic Engrg., vol. 86, 4, Dec. 1964.

15) B. Gross, J. E. Grawley, and W. F. Brown, Jr., "Stress Intensity Factors for a Single-Edge-Notch Tension Specimen by Boundary Collocation of a Stress Function", N.A.S.A.-F.N. D-2395, Lewis Research Center, August 1964.

16) G. R. Irwin, "Analysis of Stresses and Strains Near the End of a Crack Traversing a Plate", J. Appl. Mech., vol. 24, June 1957.

17) G. T. Hahn and A. R. Rosenfield, "Local Yielding and Extension of a Crack Under Plane Stress", Acta Met., vol. 13, 3, March 1965.

18) D. Laird and G. C. Smith, "Crack Propagation in High Stress Fatigue", Phil. Mag., vol. 7, 77, May 1962.

19) F. A. Field, "Yielding in a Cracked Plate Under Longitudinal Shear", J. Appl. Mech., vol. 30, 1963.

20) F. A. McClintock and G. R. Irwin, "Plasticity Aspects of Fracture Mechanics", presented at June 1964 A.S.T.M. Symposium on Crack Toughness Testing and Applications, Chicago.

21) D. R. Donaldson and W. E. Anderson, "Crack Propagation Behavior of Some Airframe Materials", Crack Propagation Symposium, Cranfield, 1961.

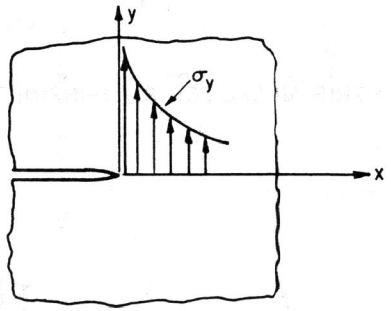

FIG.1 ELASTIC STRESSES NEAR CRACK TIP

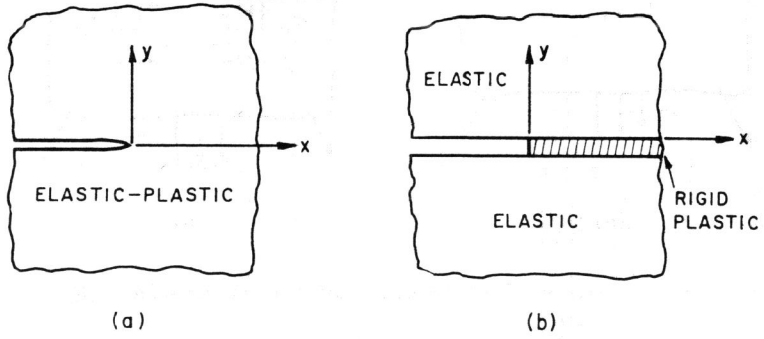

FIG.2 (a) CRACKED ELASTIC-PLASTIC BODY
(b) RIGID-PLASTIC STRIP MODEL

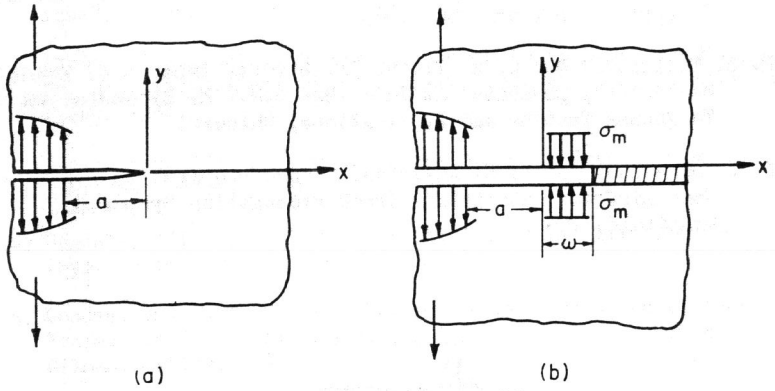

FIG. 3 STRIP MODEL FOR SEMI-INFINITE CRACK

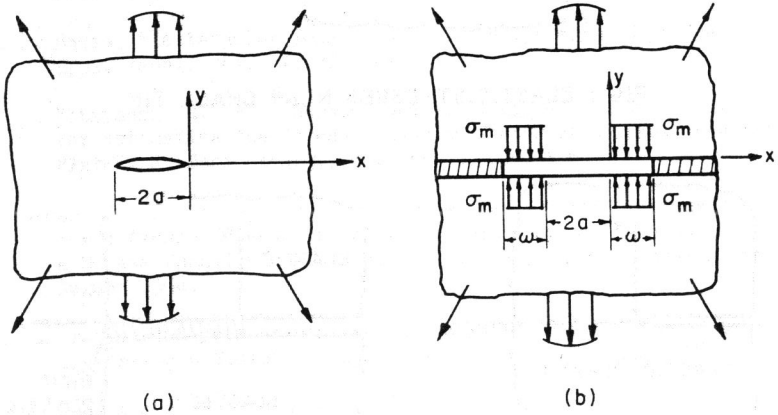

FIG. 4 STRIP MODEL FOR FINITE CRACK

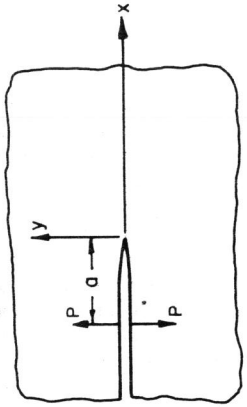

FIG. 7 SEMI-INFINITE CRACK UNDER WEDGE FORCES

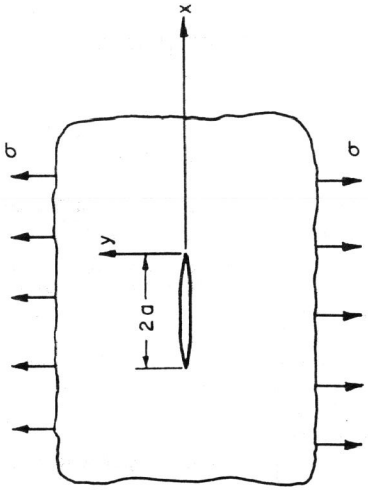

FIG. 8 FINITE CRACK IN TENSILE FIELD

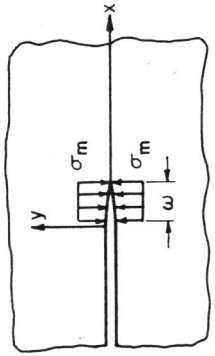

FIG. 5 EQUIVALENT ELASTIC CRACK PROBLEM FOR COMPUTATION OF $K_p^{(1)}(\omega)$ AND $F_p^{(1)}(z,\omega)$

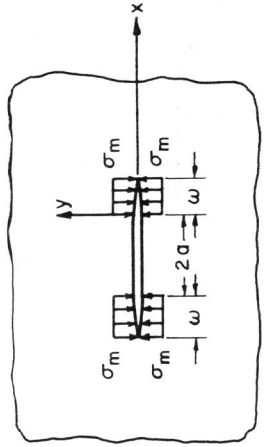

FIG. 6 EQUIVALENT ELASTIC CRACK PROBLEM FOR COMPUTATION OF $K_p^{(2)}(\omega,a)$ AND $F_p^{(2)}(z,\omega,a)$

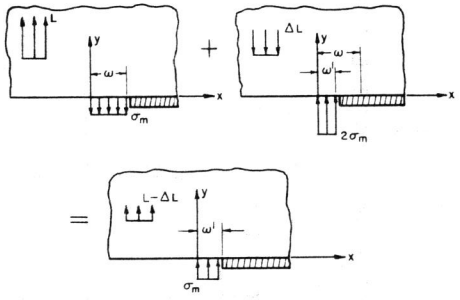

FIG. 9 SUPERPOSITIONING OF STRESS FIELDS FOR UNLOADING SOLUTION OF STRIP MODEL

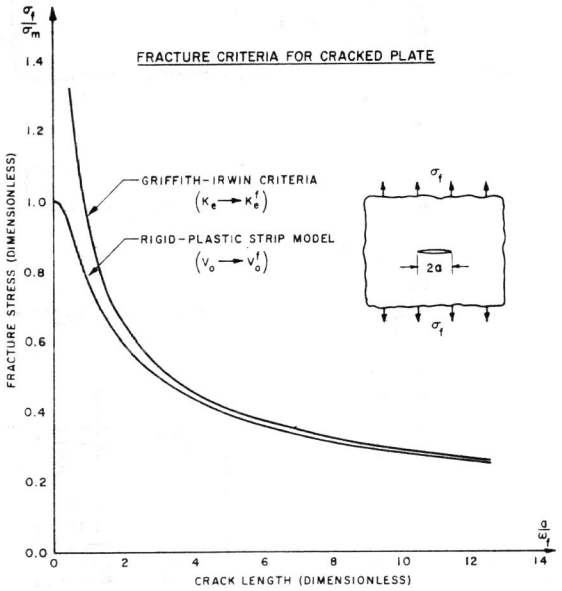

FIG. 10 COMPARISON OF FRACTURE CRITERIA